A size and space structured model describing interactions of tumor cells with immune cells reveals cancer persistent equilibrium states in tumorigenesis

Kevin Atsou[a], Fabienne Anjuère[b], Véronique Braud[b] and Thierry Goudon[a,*]

[a]Université Côte d'Azur, Inria, CNRS, LJAD, Parc Valrose, F-06108 Nice, France
[b]Université Côte d'Azur, CNRS, Institut de Pharmacologie Moléculaire et Cellulaire UMR 7275, 660 Route des Lucioles, F-06560 Valbonne, France

ARTICLE INFO

Keywords:
Tumor growth
Immune system
Equilibrium phase

ABSTRACT

The recent success of immunotherapies for the treatment of cancer has highlighted the importance of the interactions between tumor and immune cells. Mathematical models of tumor growth are needed to faithfully reproduce and predict the spatiotemporal dynamics of tumor growth. We introduce a mathematical model intended to describe by means of a system of partial differential equations the early stages of the interactions between effector immune cells and tumor cells. The model is structured in size and space, and it takes into account the migration of the tumor antigen-specific cytotoxic effector cells towards the tumor micro-environment by a chemotactic mechanism. We investigate on numerical grounds the role of the key parameters of the model such as the division and growth rates of the tumor cells, and the conversion and death rates of the immune cells. Our main findings are two-fold. Firstly, the model exhibits a possible control of the tumor growth by the immune response; nevertheless, the control is not complete in the sense that the asymptotic equilibrium states keep residual tumors and activated immune cells. Secondly, space heterogeneities of the source of immune cells can significantly reduce the efficiency of the control dynamics, making patterns of remission-recurrence appear.

1. Introduction

Cancer development is the consequence of an accumulation of mutations that leads to the deregulation of a relatively restricted number of key pathways, enough for tumor formation and progression. Tumors grow not only because of the genetic and epigenetic changes that confer a growth advantage, but also under the control of immune cells within the tumor microenvironment [19, 29]. Experimental and clinical evidences indicate that the immune system plays a critical role in the prevention and the eradication of tumors, see e. g. [19, 24, 44, 54, 55].

The genetic alterations in the tumor trigger the expression of neoantigens and upregulation of ligands of activating natural killer (NK) cell receptors which provides the immune system a basis to engage an immune response. In an efficient anti-tumor immune response, neoantigens are captured by Antigen Presenting Cells (APCs) such as Dendritic Cells (DCs) which activate naive/resting T-cells in secondary lymphoid organs draining the tumor site. As a result, activated and proliferating $CD8^+$ and $CD4^+$ effector T-cells will migrate towards the tumor micro-environment where they can eliminate tumors. This loop is known as the cancer immunity cycle, see [9]. Nonetheless, this cycle is subjected to many impediments. Succinctly, tumor antigens can be treated as self-antigens and lead to the priming of regulatory T-cells responses inhibiting effector responses [52]; tumor cells can produce inhibitory cytokines such as IL-10 or IL-4 (Interleukin 10 or Interleukin 4) which diminish the inflammation and lead to anergic and tolerant T-cells [33, 46]; tumors also express proteins such as PD-L1 which can bind to the PD-1 receptors on activated T-cells, inhibiting their cytotoxic activity [34]. Effective immune responses are thus counterbalanced by the activation of a myriad of immunosuppressive strategies [49]. The interactions between tumor cells and the immune cells rely on highly complex mechanisms, that lead to divide the immune response to cancer into three different phases: elimination, equilibrium, and escape [19]. In this context, the design of an efficient treatment by enhancing the immune response, also called immunotherapy, is challenging.

Mathematical models might help to understand the interplay between tumor growth and the immune response [12, 15, 20, 37, 50]. These models can even be completed in order to also describe and optimize the action of chemotherapy treatments and strategies to boost immune responses [2, 57]. However, most of these models are based on quite sophisticated ordinary differential equations (ODEs) systems, and do not take into account space heterogeneities, and the displacement capabilities of the immune cells. Many models also do not consider in details the uncontrolled cellular division at the origin of the tumor growth. These are the questions we address, by proposing a description based on size and space structured interacting cell populations. In this model, more specifically intended to describe the early stages of the tumor growth, the displacement of the immune cells is governed by chemotaxis, according to signals emitted by the tumor. The construction of the coupled partial differential equations (PDEs) system is based on a set of

*Corresponding author
kevin.atsou@inria.fr (K. Atsou); anjuere@ipmc.cnrs.fr (F. Anjuère); braud@ipmc.cnrs.fr (V. Braud); thierry.goudon@inria.fr (T. Goudon)
ORCID(s): 0000-0003-3144-8652 (F. Anjuère); 0000-0001-8213-3947 (V. Braud)

modeling assumptions, detailed in Section 2.1 below. These simplifying assumptions can be questionable, but they are intended to keep the most relevant mechanisms with a system of equations as simple as possible. The modeling discussion is particularly driven by the following concerns: (1) to have at hand a model affordable for numerical simulation without a too important computational cost, (2) to reduce the number of parameters: considering more intricate phenomena would require to introduce further parameters, but their role can make the discussion more obscure, due to a lack of knowledge of their effective value, and difficulty in having access to measurements [21].

The paper is organized as follows. In Section 2.1, we collect the modeling assumptions and in Section 2.2 we set up the model, which couples a convection-diffusion equation for the immune cells to a growth-fragmentation equation for the tumor cells. An overview of the main questions that are addressed with the model can be find in Section 2.3. Section 2.4 presents the mathematical insights on the equations, bringing out the capability of controlling the tumor growth, through an interpretation by means of identification of eigen-elements. The main result means that the tumor stops expanding, but it does not disappear entirely: a cancer-persistent equilibrium is reached between the tumor and the immune system, a phenomenon which has been clinically observed [10, 19, 38]. The theoretical statement assumes certain technical conditions, say on the smallness of the rate of tumor cell division, but we are not able to decide whether or not this technical restriction is necessary. Next, we investigate the features of the model on numerical grounds in Section 3. We check numerically the ability of the immune system to control tumor growth, in agreement with the theoretical result. We pay a specific attention in identifying the leading parameters that govern the immune response efficiency, which could be important to guide therapeutic strategies. Our simulations also reveal the importance of space-structuration: space heterogeneities of the sources of naive immune cells, that provide, once activated, the tumor-specific cytotoxic effector cells eliminating the tumor, dramatically influences the immune response efficiency. Replacing the homogeneous distribution of immune cells by a few spots makes the immune response less efficient. Instead of the control of the tumor, that would be kept at a fixed mass, what we can observe is a periodic succession of rapid growth and remission phases.

2. Mathematical model

2.1. Modeling assumptions

We take into account two populations of interacting cells:

- the tumor antigen-specific cytotoxic effector cells including $CD8^+$ T-cells and natural killer (NK) cells,
- the tumor cells.

The specific biological assumptions we consider to construct the model are based on the behavior of the effector cells in the micro-environment of a growing tumor and on the key phenomena governing tumor cell growth:

A.1 environmental constraints such as nutrient concentrations, temperature, etc. are assumed to be constant;

A.2 the states of the tumor cells are characterized by their size (or, equivalently, their volume or their mass);

A.3 the growth rate of a tumor cell is a deterministic process: in absence of an immune response, each tumor cell grows with a certain rate which might depend on its size;

A.4 when a tumor cell reaches a certain size, the so-called "fission size", it divides into daughter cells, usually two identical cells, at a certain rate;

A.5 each tumor cell induces a signal, for instance of chemical nature, which is related to the tumor antigenicity: the higher the mass of the tumor and the higher the antigenicity, the higher the amplitude of the signal;

A.6 the tumor antigen-specific $CD8^+$ T-cells are recruited and activated by APCs and the NK cells are recruited and activated by tumor cells from a bath of non-activated immune cells; the recruitment is characterized by a certain rate driven by the presence of tumor cells;

A.7 the activated tumor antigen-specific $CD8^+$ T-cells and the NK cells migrate towards the tumor micro-environment by chemotaxis: they follow the gradient of a potential induced by the overall tumor-derived signals;

A.8 activated tumor antigen-specific $CD8^+$ T-cells and NK cells which reach the tumor induce the death of the targeted tumor cells;

A.9 the tumor microenvironment is not immunosuppressive.

Let us discuss these assumptions, with possible hints for future developments of the modeling:

- assumption **A.1** makes sense as far as we model very early stages of tumor development. For the same reason, hypoxia effects are neglected.
- assumption **A.2** is quite restrictive. As it will be detailed below, we completely neglect any geometrical effect. It is likely that such a modeling only makes sense in the early stages of the tumor growth, when the size of the tumor remains small. Reasoning with the size of the cell is convenient to guide the intuition, but we can similarly work by characterizing the cells by the amount of cyclin complexes they contain; this leads to the same kind of equations, see [5, 6]. Moreover, many other factors can be relevant to characterize the state of a tumor cell: mutation rate, weight, age and access to nutrients, etc. It would be possible to incorporate more degrees of freedom, but it would

also raise the issue of the access to the corresponding governing parameters. For this reason, it is unclear that incorporating further details will make the model more accurate.

- assumption **A.3** can be modified by introducing some stochasticity in the growth process.
- similar considerations apply to assumption **A.4**, which can take into account random effects, or depend on further variables.
- assumptions **A.5**, **A.6** and **A.9** are restrictive too: the model is set to be in the most favorable situation to eliminate tumors but other immune cells are also involved. An important role is played by activated $CD4^+$ T cells, mostly by the IFN-γ they secrete. $CD4^+$ T-cells participate to the activation of NK cells and $CD8^+$ T-cells. But, if on the one hand the activated $CD4^+$ T-cells are stimulating the proliferation of $CD8^+$ effector T-cells, on the other hand, they can be converted into regulatory T-cells and thus limit antitumor immunity. Consequently, the immune system not only act to suppress tumor growth, but it has both stimulatory and inhibitory effects and it might fail in controlling some growing tumors, due to immunosuppressive mechanisms triggered by the tumor [10, 49, 58]. The modeling of such immunosuppressive mechanisms will be addressed in a forthcoming work. Moreover, as the tumor grow, it itself becomes more heterogeneous under the mutation dynamics, which, in turn, activates various cytotoxic responses.

2.2. Construction of the model

The model uses two distinct length scales:

- the length scale of the displacement of the immune cells. Let us denote $[L]$ the corresponding unit (typically in *mm*). Immune cells thus occupy a certain position, denoted by x and measured with $[L]$.
- the length scale of the tumor cells. Let us denote $[l]$ its unit (typically in μm). Tumor cells have a certain volume, hereafter denoted by z, measured with the unit $[l]^3$ (typically μm^3).

This modeling assumes that the length scale associated to the displacement of the immune cells is "infinitely large" compared to the length scale associated to the size of the tumor cells. It is consistent with the fact that we neglect any effects due to the geometry of the tumor, which is not sensitive at the scale of the displacement of the immune cells. The interactions between the tumor and the immune system are described by the evolution of the following unknowns:

Tumor cell density. The population of tumor cells is structured by the volume variable: $(t, z) \mapsto n(t, z)$ stands for the volumic density of tumor cells. Let $[cell_n]$ denote the unit measuring the number of tumor cells. The density n is then measured in $[cell_n] \cdot [l]^{-3}$. Given two volumes $z_2 > z_1 > 0$, the integral $\int_{z_1}^{z_2} n(t, z)\,\mathrm{d}z$ gives the number of tumor cells having a volume in the interval $[z_1, z_2]$ at time t.

The cytotoxic effector cell concentration. Let us denote $(t, x) \mapsto c(t, x)$ the concentration of immune cells that are actively fighting against the tumor (it thus includes $CD8^+$ T-cells and NK cells) at time t and position x. Let $[cell_c]$ be the unit measuring the number of immune cells. Then c is measured in $[cell_c] \cdot [L]^{-3}$. (We will perform the simulations by restricting to the two dimensional framework, assuming homogeneity in the third direction; the necessary adaptation are left to the reader.)

2.2.1. The tumor growth and division

At the macroscopic scale, the tumor is seen as a punctual mass, located, say, at the center of the region of interest ($x = 0$). The model can be easily extended to take into account multiple tumor sites. Tumor cells proliferate in an uncontrolled manner due to a loss of checkpoints of the cell cycle and they proliferate massively by staying in the mitosis phase of the cell cycle. Neglecting for the time being the interaction with the cytotoxic cells, the evolution of the tumor results from two phenomena: a natural growth and the division of mature tumor cells into daughter cells.

Let $z \mapsto V(z) \geq 0$ be the natural, possibly size-dependent, growth rate of the tumor cells. With the time variable t measured in $[t]$ (typically in day), V is measured in $[l]^3 \cdot [t]^{-1}$. At the early stages of tumor growth, see assumption **A.1**, V can be assumed constant. More intricate growth laws are presented in Appendix A.

The cell division mechanism is embodied into an operator

$$Q(n)(t, z) = -a(z)n(t, z) + \int_z^\infty a(z')k(z|z')n(t, z')\,\mathrm{d}z'. \quad (1)$$

where the gain term accounts for cells with size z produced by the division of larger cells, and the loss term is related to the division of cells with size z. The division process is governed by two quantities: the frequency $a(z')$ of division of cells having size z', thus measured in $[t]^{-1}$, and the distribution in size $k(z|z')$ of products from the division of a tumor cell with size z'. It is likely that the parameter of the division process depends on the size variable. For instance, division frequency might vanish for the smallest cells, which means $a(z) = 0$ for $0 \leq z \leq z_0$, and then be a non decreasing function of the size. The kernel k satisfies the fundamental identity [41]

$$\int_0^z z' k(z'|z)\,\mathrm{d}z' = z. \quad (2)$$

It implies the following mass conservation property

$$\begin{aligned}\int_0^\infty zQ(n)(t, z)\,\mathrm{d}z = &-\int_0^\infty za(z)n(t, z)\,\mathrm{d}z \\ &+ \int_0^\infty a(z')\left(\int_0^{z'} zk(z|z')\,\mathrm{d}z\right)n(t, z')\,\mathrm{d}z' \\ &= 0.\end{aligned}$$

For further purposes, let us introduce the expected number of cells produced from the division of a cell with size z, defined by

$$\bar{\mathcal{N}}(z) = \int_0^z k(z'|z)\,\mathrm{d}z'. \tag{3}$$

It is supposed to be larger than 1. Then, cell division changes the total number of cells by an amount given by

$$\int_0^\infty Q(n)(t,z)\,\mathrm{d}z = \int_0^\infty (\bar{\mathcal{N}}(z)-1)a(z)n(t,z)\,\mathrm{d}z \geq 0.$$

Finally, the evolution of the population of tumor cells is driven by the PDE

$$\frac{\partial}{\partial t}n(t,z) + \frac{\partial}{\partial z}(V(z)n(t,z)) = Q(n)(t,z). \tag{4}$$

referred to as a growth-fragmentation equation [41]. This type of integro-differential equation is quite common in material science and in biology [17, 18, 27, 47]; see also for specific applications to tumor growth, possibly taking into account several compartments, [5, 6]. Equation (4) is completed by the initial distribution of tumor cells

$$n\Big|_{t=0} = n_0, \tag{5}$$

and a boundary condition. Hereafter, we assume that the size variable ranges over the whole interval $(0,+\infty)$, and the boundary condition excludes the creation of cells with volume 0:

$$n(t,0) = 0. \tag{6}$$

Division and growth can be seen as competing mechanisms: the latter increases the size of the cells, while the break-up described by the former creates new smaller cells from the large ones. This can be understood by considering the evolution of the total number of tumor cells in the tumor $\mu_0(t)$ and the total volume of the tumor $\mu_1(t)$, respectively given by

$$\mu_0(t) = \int_0^\infty n(t,z)\,\mathrm{d}z, \qquad \mu_1(t) = \int_0^\infty zn(t,z)\,\mathrm{d}z. \tag{7}$$

Integrating (4) and using the boundary condition (6) yields

$$\frac{\mathrm{d}}{\mathrm{d}t}\mu_0(t) = \int_0^\infty (\bar{\mathcal{N}}(z)-1)a(z)n(t,z)\,\mathrm{d}z \geq 0, \tag{8}$$

and

$$\frac{\mathrm{d}}{\mathrm{d}t}\mu_1(t) = \int_0^\infty V(z)n(t,z)\,\mathrm{d}z \geq 0. \tag{9}$$

Equation (8) tells us that the total number of cells in the tumor increases due to cellular division processes. However, division does not influence the total volume of the tumor: we see with equation (9) that the increase of the total volume of the tumor is only due to the growth rate $V > 0$. We refer the reader to Appendix B (Table 2) for details about units and parameters for the tumor growth model.

Binary Division. A relevant example is provided by the case of binary division, where a cell with volume z splits into two cells, with respective volumes αz and $(1-\alpha)z$, $\alpha \in (0, 1/2]$ being a division parameter. The corresponding kernel reads

$$k(z'|z) = \frac{1}{\alpha}\delta_{z'=\frac{z}{\alpha}} + \frac{1}{(1-\alpha)}\delta_{z'=\frac{z}{1-\alpha}}$$

and the division operator becomes

$$\begin{aligned} Q(n)(t,z) \quad = \quad & -a(z)n(t,z) + \frac{1}{\alpha}a\Big(\frac{z}{\alpha}\Big)n\Big(t,\frac{z}{\alpha}\Big) \\ & + \frac{1}{1-\alpha}a\Big(\frac{z}{1-\alpha}\Big)n\Big(t,\frac{z}{1-\alpha}\Big). \end{aligned} \tag{10}$$

Assuming the symmetry of the division process imposes $\alpha = 1/2$ in (10), and the division operator is given by

$$Q(n)(t,z) = 4a(2z)n(t,2z) - a(z)n(t,z). \tag{11}$$

Further relevant examples of division kernels can be found in [18].

2.2.2. Evolution of the cytotoxic effector cell population

The immune cells occupy the space domain $\Omega \subset \mathbb{R}^3$. The evolution of the tumor antigen-specific cytotoxic effector cell population is driven by the mass balance principle, which leads to the local balance law

$$\partial_t c + \nabla \cdot J = S.$$

Gains and losses of cytotoxic effector cells result from two phenomena, which shape the expression of the flux J and the source S. Firstly, activated cytotoxic NK and T-cells, which can eliminate tumor cells, are extracted from a bath of non-activated immune cells. According to assumption **A.6**, the conversion of these immune cells into tumor antigen-specific effector cells depends on the mass of the tumor cells, the quantity we have already denoted $\mu_1(t)$. The description of the recruitment process involves

- $(t,x) \mapsto S(t,x)$, the space distribution of the source of immune cells (measured in $[cell_c] \cdot [L]^{-3}$). We shall observe different behaviors of the system depending whether the source S is constant or space-inhomogeneous.
- p, the, possibly space-dependent, rate at which NK and T-cells are activated (measured in $[t]^{-1}$). It takes into account the antigenicity of the tumor cells.
- a dimensionless factor $\mu_1 \mapsto g(\mu_1)$ that describes how the presence of tumor cells stimulates the production of new effector cells and the conversion of immune cells into effector cells or their recruitment. Hence, we naturally have $g(0) = 0$. Since we are treating early stages of tumor growth, we can use a mere linear relation. However, it can be relevant for longer

term interaction to impose a threshold on the recruitment process [58]. Such a saturation effect is usually taken into account with a Michaelis-Menten law [12, 39, 37], which leads to

$$g(\mu_1) = \frac{\mu_1}{\beta + \mu_1}, \tag{12}$$

where β is the steepness coefficient of the immune cell recruitment, measured in $[cell_n]$ like μ_1.

Secondly, the tumor antigen-specific cytotoxic effector cells die at a certain rate, denoted by γ. This rate can be space-dependent, or μ_1-dependent; it is measured in $[t]^{-1}$. In what follows, we will always assume that $\gamma > 0$ is constant.

Therefore, we get

$$S = g(\mu_1)pS - \gamma c.$$

We turn to the description of the tumor antigen-specific cytotoxic effector cells displacement. The motion of the cytotoxic effector cells results from two distinct phenomena. On the one hand, they follow a random walk process, that can be considered as a Brownian motion, which makes the population of activated immune cells spread in the whole domain. It is characterized by the coefficient $x \mapsto D(x)$, measured in $[L]^2 \cdot [t]^{-1}$. It can be space dependent and matrix-valued, in order to describe for instance different tissues or tissues where the displacement is easier in certain directions than in others. The details of the migration process can play a critical role in the anti-tumor immune surveillance. For instance in [51], it is reported that the fibers of the extracellular matrix control the trajectories of the cytotoxic effector cells in human lung tumors and the geometrical effects can restrict the amount of these cells infiltrating the tumor. On the other hand, a displacement towards the tumor is governed by the tumor cells antigenicity: according to assumptions **A.5** and **A.7**, the activated NK and T-cells follow the gradient of a potential, that we denote $\phi(t, x)$, induced by the tumor antigens. The directed movement of the NK and T-cells in response to the signal induced by the tumor is conditioned by the sensitivity of their membrane receptor, embodied into a factor denoted χ. It might be possible to assume that χ depends on the attractive potential ϕ, for instance to model the fact that cells do not detect signals that are too weak or too high. We can find more details about such chemotactic mechanisms in [30, 31, 32, 36]; the role of such effects in the immune response to tumor growth is already pointed out in [40]. Gathering these information, we have

$$J = \underbrace{c\chi\nabla_x\phi}_{\text{convection by chemotaxis}} - \underbrace{D\nabla_x c}_{\text{diffusion}}, \tag{13}$$

where the chemotactic velocity $\chi\nabla_x\phi$ is measured in $[L] \cdot [t]^{-1}$.

Finally, the concentration of tumor antigen-specific cytotoxic effector cells obeys the PDE

$$\partial_t c + \nabla_x \cdot (c\chi\nabla_x\phi - D\nabla_x c) = g(\mu_1)pS - \gamma c. \tag{14}$$

It is endowed by the initial data

$$c\Big|_{t=0} = c_0, \tag{15}$$

and the homogeneous Dirichlet condition

$$c\Big|_{\partial\Omega} = 0, \tag{16}$$

which means that the immune cells far from the tumor are non-activated.

2.2.3. The tumor-induced attractive potential

The attractive potential ϕ is induced by the presence of tumor cells. Every tumor cell with size z produces a certain chemical signal, according to a form function $\sigma(x, z)$. Having in mind the chemical nature of the signal, the attractive potential can be measured in number of chemoattractant molecules, with a unit denoted by $[mol]$. Accordingly, the coefficient χ will be measured in $[L]^2 \cdot [t]^{-1} \cdot [mol]$ and σ in $[mol] \cdot [cell_n]^{-1} \cdot [l]^{-3}[t]^{-1}$. The chemoattractant molecules are subjected to a natural diffusion, depending on a coefficient $\mathcal{K}$ (measured in $[L]^2 \cdot [t]^{-1}$). We can simply assume that $\mathcal{K} > 0$ is a scalar constant, but it could be a matrix-valued function of the space variable as well. The source of the attractive potential is given by the sum of all the chemical contributions of the tumor cells, which leads to the equation

$$-\nabla \cdot (\mathcal{K}\nabla\phi)(x) = \int_0^\infty zn(t, z)\sigma(x, z)\,\mathrm{d}z, \tag{17}$$

with a given matrix-valued function $x \in \Omega \mapsto \mathcal{K}(x)$ (verifying $0 < \kappa_\star \leq \mathcal{K}(x)\xi \cdot \xi \leq \kappa^\star < \infty$ for any $x \in \Omega$, $\xi \in \mathbb{S}^2$). If the form function σ does not depend on the size variable, this becomes

$$-\nabla \cdot (\mathcal{K}\nabla\phi)(x) = \sigma(x)\mu_1(t). \tag{18}$$

The equation is set on the domain Ω and needs to be completed by boundary conditions. We can choose Dirichlet boundary conditions $\phi\Big|_{\partial\Omega} = 0$. However, it is more relevant to consider instead the homogeneous Neumann condition, which tells us that the flux of chemoattractant vanishes on the boundaries of the domain

$$\mathcal{K}\nabla_x\phi \cdot \nu\Big|_{\partial\Omega} = 0. \tag{19}$$

In this case, (17), or (18), is not consistent with the boundary condition: the right hand side should be replaced by

$$\int_0^\infty zn(t, z)\sigma(x, z)\,\mathrm{d}z - \frac{1}{|\Omega|}\int_\Omega\int_0^\infty zn(t, z)\sigma(x, z)\,\mathrm{d}z\,\mathrm{d}x$$

the mean of which vanishes. In what follows we shall consider constant coefficients $\mathcal{K}$ and σ. Space inhomogeneities can be relevant to describe different conductive or sensitivity properties depending on the tissues.

2.2.4. *Effect of the immune system on the tumor*

According to assumption **A.8**, when the tumor antigen-specific cytotoxic effector cells reach the tumor micro-environment, they release cytotoxic substances which eventually leads to the death of the tumor cells. This effect is described by adding a death term in the tumor growth model (4), which becomes

$$\partial_t n + \partial_z(Vn) = Q(n) - m(c,n). \tag{20}$$

It is natural to suppose that $m(c,n)$ vanishes if either c or n vanishes. The expression of the death term involves a non negative space-dependent weight $x \mapsto \delta(x)$, measured in $[cell_n] \cdot [cell_c]^{-1} \cdot [t]^{-1} \cdot [l]^{-3}$, which incorporates both the strength of the immune response and a radius of interaction. This weight might equally depend on the tumor volume $t \mapsto \mu_1(t)$. Inspired from [37] the death term can be modeled by Michealis-Menten kinetics:

$$m(c,n)(t,z) = \int_\Omega \delta(y)c(t,y)\,\mathrm{d}y \times \frac{1}{\alpha} \times \frac{n(t,z)}{1+\alpha' n(t,z)}, \tag{21}$$

with $\alpha, \alpha' > 0$, but we shall also work with a linear expression (which amounts to set $\alpha' = 0$). Further details on the units of the parameters of the equations can be found in Appendix B (Table 3).

2.3. Summary and workplan

The general interaction model we are dealing with thus reads (for $t \geq 0$, $z \geq 0$, $x \in \Omega$)

$$\begin{cases} \partial_t n + \partial_z(Vn) = Q(n) - m(c,n), \\ \partial_t c + \nabla_x \cdot (c\chi\nabla_x\phi - D\nabla_x c) = pg(\mu_1)S - \gamma c, \\ -\nabla\cdot(\mathcal{K}\nabla\phi) = \displaystyle\int_0^\infty zn(t,z)\sigma(x,z)\,\mathrm{d}z \\ \qquad\qquad -\dfrac{1}{|\Omega|}\displaystyle\int_\Omega\int_0^\infty zn(t,z)\sigma(x,z)\,\mathrm{d}z\,\mathrm{d}x, \\ n(t,0) = 0 \text{ for } t \geq 0, \\ n(t=0,z) = n_0(z) \text{ for } z \geq 0, \\ c(t,x) = 0 \text{ for } x \in \partial\Omega, \\ c(t=0,x) = c_0(x) \text{for } x \in \Omega, \\ \mathcal{K}\nabla\phi\cdot\nu = 0 \text{ for } x \in \partial\Omega. \end{cases} \tag{22}$$

We remind the reader that the cell division operator $Q(n)$ and the immune cell-tumor interaction term $m(c,n)$ are defined in (1) and (21) respectively. We refer the reader to Tables 2 and 3 where the biological meaning of the unknowns and of the parameters is recapitulated.

We shall see that the model (22) is able to reproduce equilibrium states, where the tumor and the effector cells are in a dynamic balance, and we will provide a mathematical justification of this fact (see Theorem 2 below). In the equilibrium phase, as pointed out in [19], tumor cell proliferation appears to be controlled by the immune system and we address on numerical grounds the effects that influence this control. In particular, the mass of the residual tumor and the speed of convergence to the equilibrium state can vary significantly with the parameters of the model. Accordingly, we particularly challenge the following effects:

- dealing with a space-structured model gives access to new phenomena: we will compare the homogeneous distribution of the source of naive immune cells to the case where the cells are heterogeneously distributed at a certain distance of the micro-environment of the tumor.
- it is important to determine how the parameters influence the dynamics, not only through their strength, but also depending whether or not they depend on the size or space variables: On the one hand, the aggressiveness of the tumor can be tested by acting on the growth rate V and on the division rate a of the tumor cells. On the other hand, the efficiency of the host immune system depends on the activation rate p, the death rate γ, the immune strength δ and the migration of NK and T-cells towards the tumor microenvironment. Note also that immunotherapy can modify these parameters, for instance by improving tumor elimination through increasing cytotoxic strength (that can be achieved by acting on anti-immune checkpoint like PD-1) [58], by fostering T-cells enrichment, as a consequence of the depletion of $Gr1+$ cells, or by blocking myeloid suppressor cell recruitment to the tumor site [23, 28, 35].
- as said above, saturation effects can be taken into account in both the conversion process of immune cells into tumor antigen-specific cytotoxic effector cells and the death of tumor cells by these cytotoxic cells. We will discuss the role of these saturation effects on the dynamics, comparing the saturated and non-saturated models in Appendix D.

2.4. A few mathematical comments

This Section aims at providing an intuition on the behavior of the solutions of (22), based on mathematical arguments. First, with some simplifying assumptions, the equations can be reduced to a mere ODEs system, which admits stationary solutions. The stability analysis helps in understanding the role of the parameters of the model. Second, by means of eigen-elements of the cell division equation, we identify a scenario which reproduces the equilibrium phase of the tumor-immune interaction [19].

2.4.1. *A simplified model: damping and oscillations*

Under some restrictive assumptions, we can obtain a closed set of ODEs by integrating (22) over the size and space variables. This (oversimplified) situation shed some light on the role of the parameters. Let us consider the very specific case where

- the source S of immune cell is constant,
- all parameters V, δ, p, $\mathcal{K}$ are constant,

- σ does not depend on the size variable,
- the interactions are non saturated: $m(c,n) = \delta n \int_\Omega c\,\mathrm{d}y$, and $g(\mu_1) = \mu_1$,
- we consider the binary division model, as described in (11), with a constant frequency a.

Moreover, we replace the homogeneous Dirichlet boundary condition (16) for the NK and T-cells by the Neumann boundary condition

$$\nabla c \cdot \nu\Big|_{\partial\Omega} = 0. \tag{23}$$

These assumptions clearly lack of biological relevance. For instance, assuming that a and δ are constant means that any tumor cell has the same division rate a, irrespective of its size, and any effector cell acts the same way on the tumor, irrespective of its position in the domain Ω. The resulting model reads

$$\begin{cases} \big(\partial_t n + \partial_z(Vn)\big)(t,z) \\ \qquad = -an(t,z) + 4an(t,2z) - \delta n(t,z)\displaystyle\int_\Omega c(t,y)\,\mathrm{d}y, \\ \partial_t c + \nabla_x \cdot (c\chi\nabla_x\phi - D\nabla_x c) = p\mu_1 S - \gamma c, \\ -\mathcal{K}\Delta_x\phi = \mu_1\langle\sigma\rangle, \\ n(t=0,z) = n_0(z),\ c(t=0,x) = c_0(x), \\ n(t,0) = 0,\ \nabla_x c\cdot\nu(t,\cdot)\Big|_{\partial\Omega} = 0,\ \nabla_x\phi\cdot\nu(t,\cdot)\Big|_{\partial\Omega} = 0, \end{cases} \tag{24}$$

where we use the shorthand notation $\langle\sigma\rangle = \sigma - \frac{1}{|\Omega|}\int_\Omega \sigma\,\mathrm{d}x$. As simple as it appears, this model can provide useful hints on the qualitative features of the original PDEs system. In this simple framework, the dynamics can be understood by considering a reduced system of ODEs. Indeed, we obtain a closed system of equations for μ_0, μ_1, given by (7), and the total number of active immune cells

$$\mu_c(t) = \int_\Omega c(t,x)\,\mathrm{d}x.$$

We get

$$\begin{cases} \dfrac{\mathrm{d}}{\mathrm{d}t}\mu_0 = \mu_0\left(a - \delta\mu_c\right), \\ \dfrac{\mathrm{d}}{\mathrm{d}t}\mu_1 = V\mu_0 - \delta\mu_1\mu_c, \\ \dfrac{\mathrm{d}}{\mathrm{d}t}\mu_c = \pi pS\mu_1 - \gamma\mu_c. \end{cases} \tag{25}$$

The states

$$\begin{pmatrix}\mu_0^H\\ \mu_1^H\\ \mu_c^H\end{pmatrix} = \begin{pmatrix}0\\0\\0\end{pmatrix}, \qquad \begin{pmatrix}\mu_0^{UH}\\ \mu_1^{UH}\\ \mu_c^{UH}\end{pmatrix} = \begin{pmatrix}\dfrac{\gamma a^2}{\pi\delta V pS}\\ \dfrac{\gamma a}{\pi\delta pS}\\ \dfrac{a}{\delta}\end{pmatrix}$$

are equilibrium solutions of (25). The former corresponds to an healthy state, the latter to a stationary state with residual tumors and immune cells. For the unhealthy state, the more important the bath of immune cells or the recruitment probability, the lesser the tumor mass; the more agressive the tumor (with a higher division rate a) or the weaker the immune system, the higher the tumor mass.
The Jacobian matrix evaluated at the equilibrium points reads

$$J^H = \begin{pmatrix} a & 0 & 0 \\ V & 0 & 0 \\ 0 & \pi pS & -\gamma \end{pmatrix}, \quad J^{UH} = \begin{pmatrix} 0 & 0 & -\dfrac{\gamma a^2}{\pi V pS} \\ V & -a & -\dfrac{\gamma a}{\pi pS} \\ 0 & \pi pS & -\gamma \end{pmatrix},$$

respectively. Therefore, as far as the cell division is active ($a > 0$), J^H has a positive eigenvalue and the healthy state is unstable. For the unhealthy state, the characteristic polynomial is $p(\lambda) = -\lambda^3 - (a+\gamma)\lambda^2 - 2a\gamma\lambda - \gamma a^2$. We distinguish two cases, driven by the ratio $\frac{\gamma}{a}$ ($=\frac{\text{death rate of immune cells}}{\text{tumor cells division rate}}$)

- if $\gamma > 4a$, the eigenvalues are real; they are given by

$$\lambda_1 = -a, \quad \lambda_2 = \frac{1}{2}\left(-\sqrt{\gamma(\gamma-4a)} - \gamma\right), \\ \text{and } \lambda_3 = \frac{1}{2}\left(\sqrt{\gamma(\gamma-4a)} - \gamma\right),$$

  and they are all negative.

- if $\gamma < 4a$, the eigenvalues have an imaginary part:

$$\lambda_1 = -a, \quad \lambda_2 = \frac{1}{2}\left(-i\sqrt{\gamma(4a-\gamma)} - \gamma\right), \\ \text{and } \lambda_3 = \frac{1}{2}\left(i\sqrt{\gamma(4a-\gamma)} - \gamma\right),$$

  but all the real parts are negative: $\lambda_1 < 0$, $\mathrm{Re}(\lambda_2) = \mathrm{Re}(\lambda_3) = -\frac{\gamma}{2} < 0$.

Therefore, the unhealthy state is always stable. The asymptotic behavior of the solution depends only the ratio γ/a: $\gamma = 4a$ is a threshold between a purely damped behavior, see Fig. 1 and 2-(a), (b), (c), and an oscillatory behavior (the greater the cell division, the faster the oscillations), see Fig. 1 and 2-(d), (e), (f). These oscillations thus appear when the tumor is more aggressive, while the damping rate is driven by the immune efficiency.

2.4.2. Existence of equilibrium phases

Let us go back to the growth-fragmentation equation (4), with a general division process described by (1), with possibly size-dependent division frequency $z \mapsto a(z)$ and growth rate $z \mapsto V(z)$, respectively, neglecting for a while the immune response. The large time behavior of the cell division equation is described by means of eigen-elements of the transport-division operator. Namely, we seek a positive function $z \geq 0 \mapsto N(z) \geq 0$ and a positive number $\lambda > 0$ such that

$$\begin{cases} \partial_z(VN) - Q(N) + \lambda N = 0 \text{ for } z \geq 0, \\ N(0) = 0,\ N(z) > 0 \text{ for } z > 0,\ \displaystyle\int_0^{+\infty} N(z)\,\mathrm{d}z = 1. \end{cases}$$

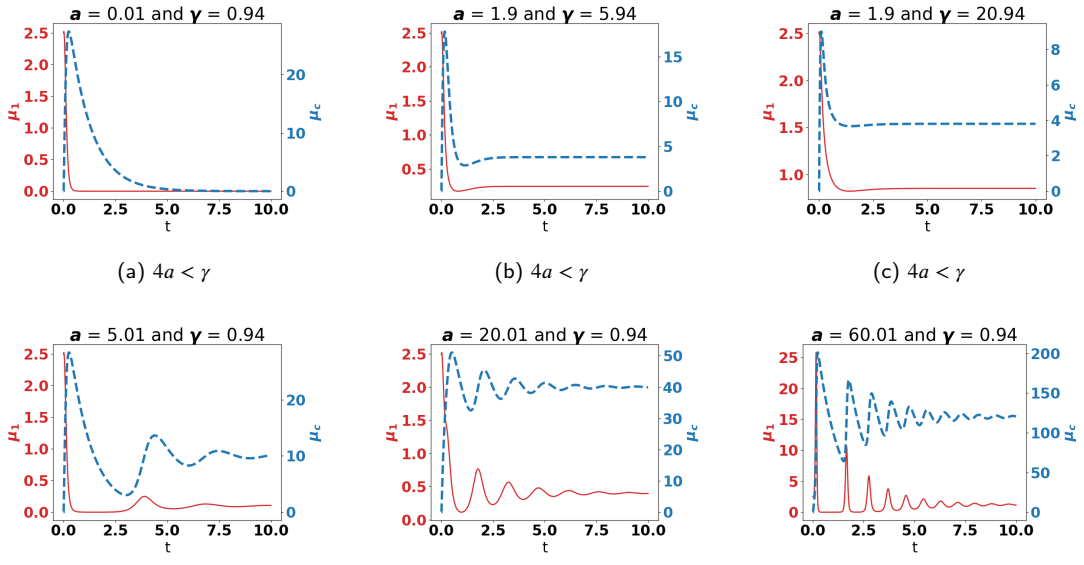

(a) $4a < \gamma$ (b) $4a < \gamma$ (c) $4a < \gamma$

(d) $4a > \gamma$ (e) $4a > \gamma$ (f) $4a > \gamma$

Figure 1: Typical behavior of the solutions of (25). The data are: $V = 0.616$, $\delta = 0.5$, $p = 4.66$, $S = 6.38$ (x-axis: time, y-axis: μ_1, mass of the tumor, and μ_c, the total number of active immune cells).

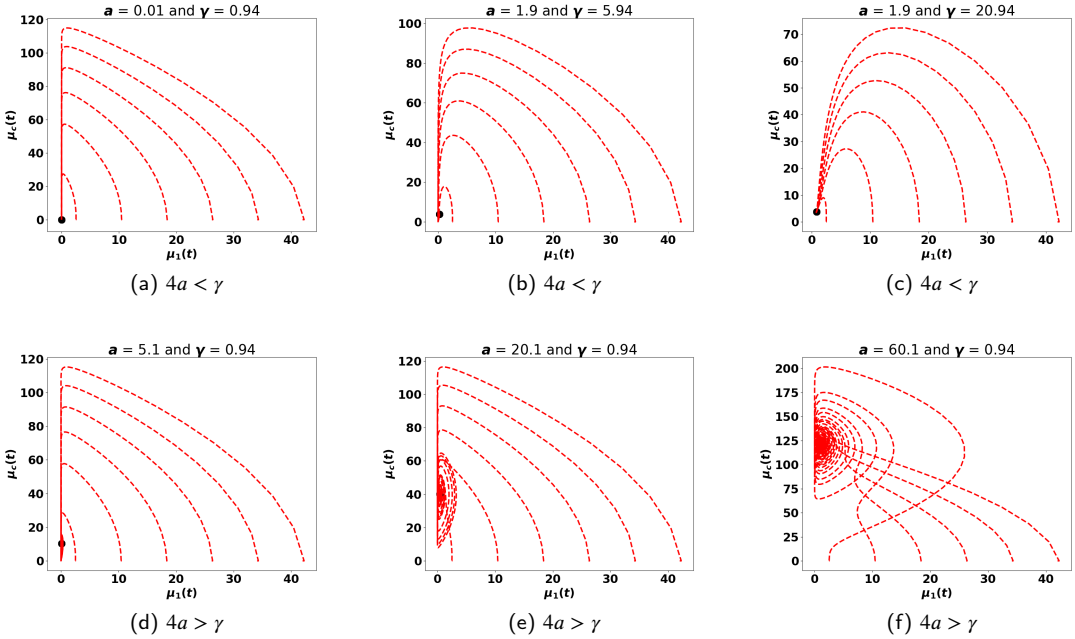

(a) $4a < \gamma$ (b) $4a < \gamma$ (c) $4a < \gamma$

(d) $4a > \gamma$ (e) $4a > \gamma$ (f) $4a > \gamma$

Figure 2: Typical phase portraits (μ_1, μ_c) of (25) for different initial tumor mass. The data are: $V = 0.616$, $\delta = 0.5$, $p = 4.66$, $S = 6.38$

(26)

The analysis of this eigen-problem requires some technical assumptions. For instance, when the growth rate V is constant, we suppose:

(H1) $a \in L^\infty((0,\infty))$ and there exists $z_\star \geq 0, \alpha^\star \geq \alpha_\star > 0$ such that $0 \leq a(z) \leq \alpha^\star$ for any $z \geq 0$, $0 < \alpha_\star \leq a(z)$ for any $z \geq z_\star$,

(H2) $k(z|z') \geq 0$, $k(z|z') = 0$ when $z' < z$ and

$$\int_0^\infty z k(z|z')\,\mathrm{d}z = z'.$$

These assumptions ensure the existence-uniqueness of the eigenpair (λ, N), satisfying (26), see [42] and the textbook [47, Theorem 4.6] which indicates further connections with the renewal equation. The case where the growth rate V is non-constant is addressed in [18]; the assumptions necessary for the analysis are collected in Appendix A. Then, it can be shown that $n(t, z)$ behaves as time becomes large like $e^{\lambda t}\rho N(z)$, where $\rho > 0$ is entirely determined by the initial condition n_0: see [43] where this result is established by using relative entropy techniques (and [14] for a very similar problem arising in tumor growth modeling too).

The precise expression of the eigen-function N is not explicitly known in general. Nevertheless, for the specific kernel of symmetric binary division, see (11), with a constant division rate we have detailed information, as shown in [4], see also [48] and [47, Lemma 4.1].

Lemma 1. *Let Q be defined by (11) with a constant division rate $a > 0$. Let V be a positive constant. Let $(\alpha_n)_{n\in\mathbb{N}}$ be the sequence defined by the recursion*

$$\alpha_0 = 1, \qquad \alpha_n = \frac{2}{2^n - 1}\alpha_{n-1}.$$

Then the function

$$N(z) = \bar{N}\sum_{n=0}^{\infty}(-1)^n\alpha_n \exp\left(-2^{n+1}\frac{a}{V}z\right),$$

with $\bar{N} > 0$ an appropriate normalizing constant, belongs to the Schwartz class $\mathcal{S}(\mathbb{R}^+)$ and is the unique solution of (26), where $\lambda = a$.

The shape of the profile is governed by the ratio $\frac{a}{V}$ ($= \frac{\text{division rate}}{\text{growth rate}}$), as illustrated by Fig. 3: the smaller the division rate (resp. the higher the growth rate), the more spread the profile. According to the intuition a large growth rate promotes the formation of large tumor, a large division rate favors the proliferation of small cells.

This (semi-)explicit formula will be used to check numerically the behavior of the coupled problem when it tends to a stationary state. For general fragmentation kernels, we can obtain the following relation: integrating (26) over $z \in (0, \infty)$ yields

$$\lambda = \int_0^\infty Q(N)\,\mathrm{d}z = \int_0^\infty (\bar{\mathcal{N}}(z) - 1)a(z)N(z)\,\mathrm{d}z$$

with $\bar{\mathcal{N}}$ defined in (3) (which tells us that $\lambda = a$ for (11) with a constant division rate). Similarly, considering the first order moment of the equation, we get

$$\lambda = \frac{\displaystyle\int_0^\infty V N(z)\,\mathrm{d}z}{\displaystyle\int_0^\infty z N(z)\,\mathrm{d}z}. \tag{27}$$

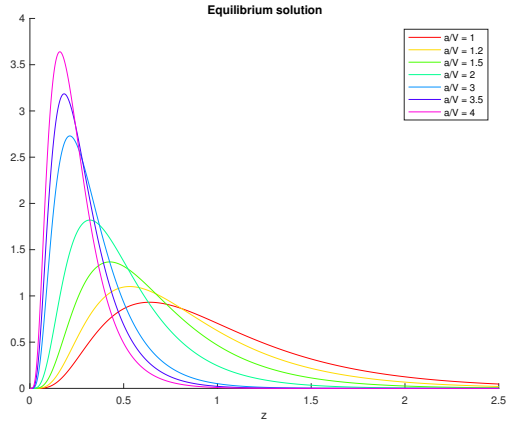

Figure 3: Shape of the leading eigen-function of the growth-division equation for several values of $\frac{a}{V}$ (x-axis: z, size of the tumor cells, y-axis: number of tumor cells at the final time)

Now, we turn back to the coupled system (22): these considerations will be crucial to discuss the large time behavior of the system. Precisely, we consider the version where

- there is no saturation in the death rate induced by the interaction,
- σ depends only on the space variable x.

Namely, we have

$$\begin{cases} \partial_t n + \partial_z(Vn) = Q(n) - n\displaystyle\int_\Omega \delta(x)c(t,x)\,\mathrm{d}x \\ \partial_t c + \nabla_x\cdot(\chi c\nabla_x\phi - D\nabla_x c) = pg(\mu_1)S - \gamma c, \\ -\nabla_x\cdot(\mathcal{K}\nabla_x\phi) = \mu_1\langle\sigma\rangle \\ n(t=0,z) = n_0(z),\ c(t=0,x) = c_0(x) \\ n(t,0) = 0,\ c(t,\cdot)\big|_{\partial\Omega} = 0,\ \mathcal{K}\nabla_x\phi(t,\cdot)\big|_{\partial\Omega} = 0. \end{cases}$$

Here, we assume

- $\mathcal{K}$, D are bounded matrix-valued functions defined on Ω, that verify a uniformly elliptic condition,
- V, a and k are such that (26) admits a unique solution,
- $g : [0,\infty) \mapsto [0,\infty)$ is a C^1 increasing function such that $g(0) = 0$,
- $x \mapsto pS(x)$ and $x \mapsto \sigma(x)$ are non negative functions that belong to $L^2(\Omega)$.

We observe in the numerical experiments that in many situations, a non proliferation state can be reached and the integral $\int_\Omega \delta(y)c(t,y)\,\mathrm{d}y$ tends to a constant. We wish to provide a mathematical explanation of this phenomenon, which corresponds to the equilibrium phase clinically observed [10,

19, 38], with residual tumors and active immune cells. A natural candidate for the tumor size-distribution is an equilibrium $\bar{\mu}_0 N(z)$, with N the eigen-function defined by (26). Thus, we wish to identify a stationary solution of (22) under the form $(\bar{\mu}_0 N(z), \bar{C})$. This leads to the relation

$$\underbrace{\big(\partial_z(V\bar{\mu}_0 N) - Q(\bar{\mu}_0 N)\big)(z)}_{=-\lambda\bar{\mu}_0 N(z)} = -\bar{\mu}_0 N(z)\int_\Omega \delta(x)\bar{C}(x)\,\mathrm{d}x.$$

Hence, the concentration of cytotoxic effector cells should satisfy

$$\int_\Omega \delta(x)\bar{C}(x)\,\mathrm{d}x = \lambda,$$

the leading eigenvalue of the (free-)fragmentation equation. This can be checked on the numerical simulations, for the simplified division model (11) with a constant division rate $a > 0$, and working with a constant growth rate V: we find that $\int_\Omega \delta(y)c(t,y)\,\mathrm{d}y$ tends to a, and $n(t,z)$ becomes proportional to the profile given in Lemma 1. Therefore, we expect that the immune system organizes so that the death rate induced by the action of the cytotoxic effector cells counterbalances the natural Malthusian behavior of the cell division equation. That the death rate can, in certain circumstances, reaches the leading eigenvalue of the cell division equation is justified by the following statement.

Theorem 2. *Let Φ be the solution of*

$$-\nabla_x\cdot(\mathcal{K}\nabla_x\Phi) = \sigma - \frac{1}{|\Omega|}\int_\Omega \sigma(y)\,\mathrm{d}y,$$

endowed with the homogeneous Neumann boundary condition. If $\ell > 0$ is small enough, there exists a unique $\bar{\mu}_1(\ell) > 0$ such that $C_{\bar{\mu}_1(\ell)}$, solution of the stationary equation

$$\begin{cases} \gamma C - \nabla_x\cdot(D\nabla_x C) - \bar{\mu}_1\nabla_x\cdot(C\nabla_x\Phi) = g(\bar{\mu}_1)pS, \\ C\Big|_{\partial\Omega=0} = 0, \end{cases} \tag{28}$$

satisfies $\int_\Omega \delta C\,\mathrm{d}x = \ell$.

Proof. We introduce the mapping

$$\mathscr{F} : (\ell,\mu_1)\in[0,\infty)\times[0,\infty) \longmapsto \int_\Omega \delta C_{\mu_1}\,\mathrm{d}x - \ell$$

where C_{μ_1} is the solution of (28) associated to μ_1. We are searching for the zeroes of $\mathscr{F}$. Of course $\mathscr{F}(0,0) = 0$, with $C_0 = 0$. Next, we have $\partial_{\mu_1}\mathscr{F}(\ell,\mu_1) = \int_\Omega \delta C'_{\mu_1}\,\mathrm{d}x$, with C'_{μ_1} the solution of

$$\begin{cases} \gamma C' - \nabla_x\cdot(D\nabla_x C') - \mu_1\nabla_x\cdot(C'\nabla_x\Phi) \\ \qquad\qquad = g'(\mu_1)pS + \nabla_x\cdot(C_{\mu_1}\nabla_x\Phi), \\ C'\Big|_{\partial\Omega=0} = 0. \end{cases}$$

In particular, since $g'(0)pS \neq 0$ is non negative and $C_0 = 0$, the maximum principle for elliptic equations tells us that $C'_0 > 0$. It follows that $\partial_{\mu_1}\mathscr{F}(0,0) = \int_\Omega aC'_0\,\mathrm{d}x > 0$. We can thus apply the implicit function theorem: there exists $\ell_\star > 0$ and a mapping $\bar{\mu}_1 : \ell\in[0,\ell_\star) \mapsto \bar{\mu}_1(\ell)$ such that for any $\mathscr{F}(\ell,\bar{\mu}_1(\ell)) = 0$ holds for any $\ell\in[0,\ell_\star)$. We have

$$\begin{aligned}\partial_\ell\mathscr{F}(\ell,\bar{\mu}_1(\ell)) + \bar{\mu}'_1(\ell)\partial_{\mu_1}\mathscr{F}(\ell,\bar{\mu}_1(\ell)) \\ = -1 + \bar{\mu}'_1(\ell)\partial_{\mu_1}\mathscr{F}(\ell,\bar{\mu}_1(\ell)) = 0\end{aligned}$$

with $\partial_{\mu_1}\mathscr{F}(0,0) > 0$. Hence, $\ell\mapsto\bar{\mu}_1(\ell)$ is increasing on the neighborood of $\ell = 0$, and it thus takes positive values. ∎

We remind the reader that the asymptotic behavior for the tumor population is expected to be described by an eigenfunction associated to the leading eigenvalue λ, thus proportional to $z\mapsto N(z)$. Theorem 2 defines implicitly the corresponding value $\bar{\mu}_1$ of the total mass, and we can find $\bar{\mu}_0$ accordingly (for instance, when V is constant, by going back to (27) we get $\lambda = V\frac{\bar{\mu}_0}{\bar{\mu}_1}$). Theorem 2 applies when the leading eigenvalue is small enough. For the simple binary division model (11) with a constant division rate a, according to Lemma 1, this is a smallness assumption on a. Therefore this statement raises the following questions that will be investigated numerically: (1) is this condition only a technical requirement ? how small should be a to observe a control and what happens as a becomes large ? (2) how μ_1, the total mass of the persistent tumor, behaves with respect to the parameters ? These issues can be interpreted as indicators of the efficiency of the immune response. In a forthcoming work, we shall investigate how this approach permits us to compute *a priori* the equilibrium state and the mass of the residual tumor that can be predicted for a given set of parameters [3].

3. Results of the numerical experiments

In what follows, the tumor is always located at the origin of the computational domain Ω, which is the ball $\Omega = \{x = (x_1,x_2)\in\mathbb{R}^2, |x| = \sqrt{x_1^2+x_2^2} < R\}$. (Of course, simulations can be performed in 3D as well, up to an increase of the computational cost.) The simplification discussed in Section 2.4.1 is very specific: it does not hold when changing the boundary condition for c and taking into account the fact that the action of the cytotoxic cells is localized. To this end, we use a weight δ, which is a Gaussian centred at $x = 0$ with a fixed variance θ and an amplitude A:

$$\delta(x) = \frac{A}{\theta\sqrt{2\pi}}\exp\left(-\frac{|x|^2}{2\theta^2}\right). \tag{29}$$

For defining the source term of the chemoattractant potential, we also use a Gaussian profile

$$\sigma(x) = \frac{A_\sigma}{\theta_\sigma\sqrt{2\pi}}\exp\left(-\frac{|x|^2}{2\theta_\sigma^2}\right). \tag{30}$$

Throughout this Section, we assume that the interaction term has the form:

$$m(c,n)(t,z) = n(t,z)\int_\Omega \delta(y)c(t,y)\,\mathrm{d}y$$

and $g(\mu_1) = \mu_1$. In order to ease comparison, we make use of the binary division operator, so that we will compare the asymptotic size-distributions of tumors with the profile given by Lemma 1. Appendix C provides details about the numerical method used to perform the simulations. For the simulations, we shall use the following data, otherwise explicitly stated: the initial data are $E_0(x) = 0$ and $n_0(z) = \mathbf{1}_{0\le z\le 750}$ and the parameters are given in Table 1.

3.1. Homogeneous distribution of the source of immune cells: an equilibrium state with persistent tumors establishes

We start by considering the case where the source of immune cells is homogeneously distributed which means that S is constant over the domain Ω. This assumption is relevant for the NK cells.

The fundamental observation is that the size-distribution of tumors tends to the profile given in Lemma 1, see Fig. 4. The chemotactic potential, and the concentration of activated cytotoxic cells also tend to stationary states: the former points towards the center of the domain where the tumor is located, see Fig. 5, the latter is more concentrated at the center of the domain, see Fig. 6. In Fig. 7–11, we show the evolution of the mass μ_1 of the tumor compared to the immune strength $\bar\mu_c(t) = \int_\Omega \delta(x)c(t,x)\,\mathrm{d}x$, for different values of the parameters. Depending on the values of the parameters, we observe some damped oscillations in the tumor mass and in the concentration of immune cells. We observe that, when the tumor mass decreases, the tumor antigen-specific cytotoxic effector cells take more time to leave the tumor micro-environment. This latter phenomenon is converted into a slight delay in the time evolution of the cytotoxic effector cells concentration in the tumor micro-environment with respect to the evolution of the tumor mass when both of them are decreasing. According to what is expected from Theorem 2, $\bar\mu_c(t)$ tends to a, the leading eigenvalue of the free-growth/division equation; this is a robust observation of the numerical investigation.

Next, we make the parameters vary in order to discuss the influence of their value on the behavior of the system. We only modify one quantity at a time, the others being kept as in Table 1.

- *Tumor aggressiveness.* By increasing the rate division a we make the tumor more aggressive, see Fig. 7. We recover a qualitative behavior observed in Section 2.4.1: for small a's the mass of the tumor is rapidly damped, and oscillation-free. An oscillatory behavior can be observed as a increases: the higher a, the higher the frequency. For the tested parameters, the damping always occurs, with a convergence towards the expected asymptotic profile. The asymptotic mass of tumor is significantly positive for large a. We observe that the tumor mass reaches higher values when a is larger, both during the transient states and for the equilibrium value. Note also that the profile of the time evolution becomes sharper, especially for the reaction of the immune system, see (d): $\bar\mu_c$ increases rapidly in response to a growth of the tumor mass, and, once the tumor controlled, it relaxes gently.

  Consistently with Section 2.4.1, as the immune cell death rate γ decreases, oscillations appear. Note also that the value of γ impacts significantly the asymptotic value of the mass of the tumor: the higher γ, the higher the tumor mass, see Fig. 8.

- *Efficiency of the immune response.* The immune response is enhanced by increasing either A, the amplitude of the death term in the tumor growth equation (it measures the strength of the immune cells against the tumor cells), see (29), or the conversion rate p: this sensitively reduces the final amount of tumors, and slightly accelerates the damping, see Fig. 9.

  The immune response is also influenced by playing on the strength of the chemoattractive effect (by increas-

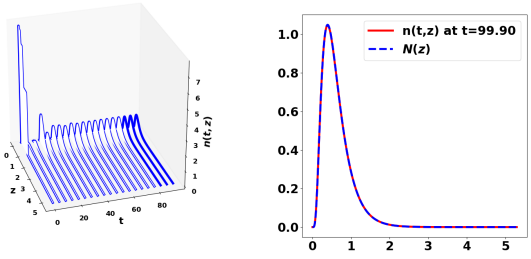

Figure 4: Convergence to the asymptotic profile. Left: Time evolution of the tumor profile. Right: Comparison of the tumor size-distribution at $T = 99.90$ with the exact asymptotic state (x-axis: z, size of the tumor cells, y-axis: number of tumor cells at the final time)

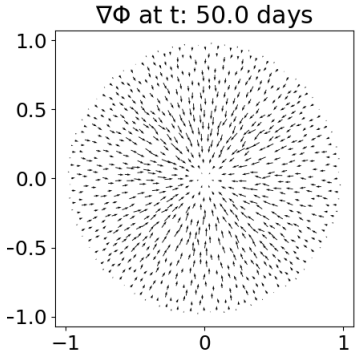

Figure 5: Non saturated interactions, homogeneous source of immune cells: the gradient of the chemotactic potential at $t = 50.0$ (the axis correspond to the space coordinates)

R	A	θ^2	A_σ	θ^2_σ	a	V	p	χ	S	γ
1	1	0.02	0.002	0.05	0.8	0.616	0.25	0.864	20	0.18

Table 1
Data for the simulations

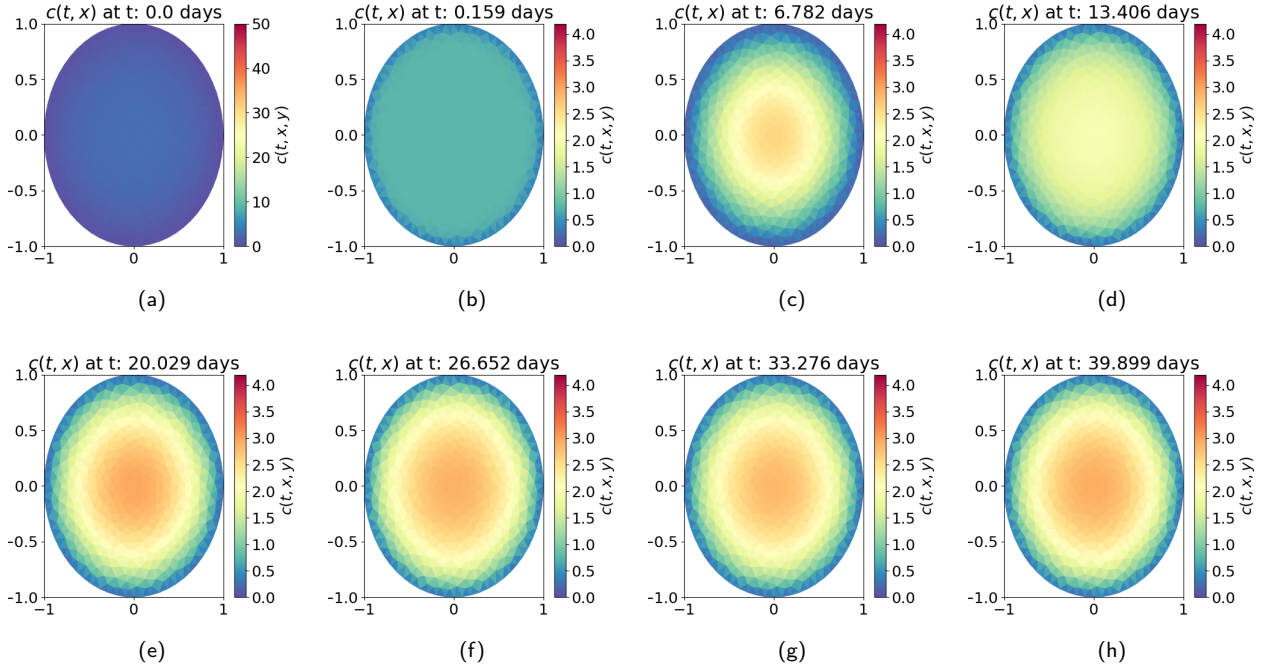

Figure 6: Non saturated interactions, homogeneous source of immune cells: time evolution of the cytotoxic effector cells concentration c (the axis correspond to the space coordinates)

ing χ or A_σ). The amplitude A_σ represents the amplitude of the tumor antigenicity, see (30). It is well known that the more antigenic a tumor, the more effective the immune response. Quite surprisingly, the effect is not that sensitive: by increasing A_σ oscillations are slightly smoothed out and the convergence to the asymptotic profile is a bit faster, see Fig. 10. What is much more important is the diffusion coefficient D: increasing D dramatically reduces the efficiency of the immune system: an asymptotic profile is still reached, but the equilibrium tumor mass can be significantly higher, see Fig. 11 (note it it is not monotone with respect to D). This observation raises the issue of considering space dependent diffusion coefficients, possibly matrix valued, describing more or less favorable spreading conditions depending on the tissues surrounding the tumor.

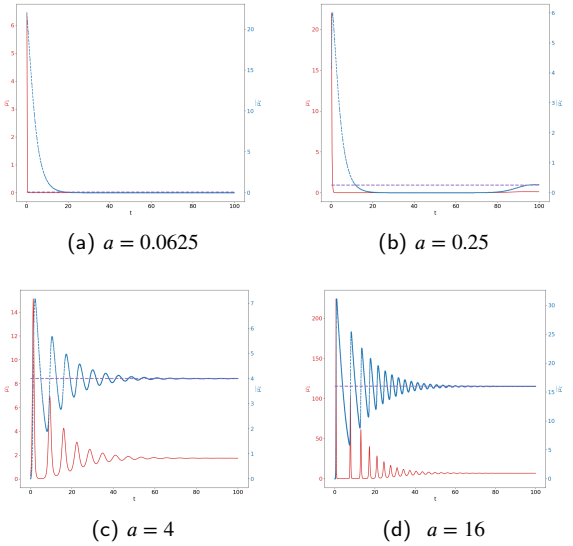

(a) $a = 0.0625$ (b) $a = 0.25$

(c) $a = 4$ (d) $a = 16$

Figure 7: Non saturated interactions, homogeneous source of immune cells. Evolution of the tumor mass μ_1 (red curves, left axis), and of $\bar{\mu}_c$ (blue curve, right axis) for several values of the division rate a

3.2. Influence of space-heterogeneities: equilibrium states vs. periodic behavior

In this Section, we keep the same model and data as in Table 1, but we deal with a non homogenous source of immune cells, see Fig. 12. This situation is biologically related to the action of the T-cells. It describes the fact that non-

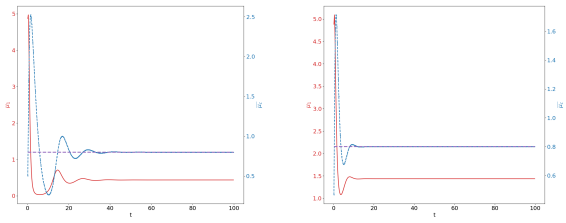

(a) $\gamma = 0.0625$ (b) $\gamma = 0.25$

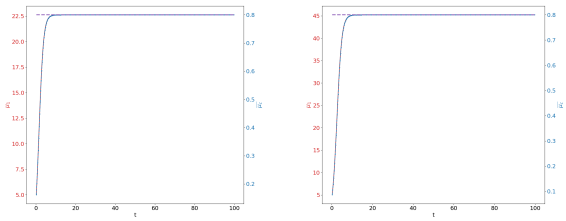

(c) $\gamma = 1$ (d) $\gamma = 16$

Figure 8: Non saturated interactions, homogeneous source of immune cells. Evolution of the tumor mass μ_1 (red curves, left axis), and of $\bar{\mu}_c$ (blue curve, right axis) for several values of the immune cells death rate γ

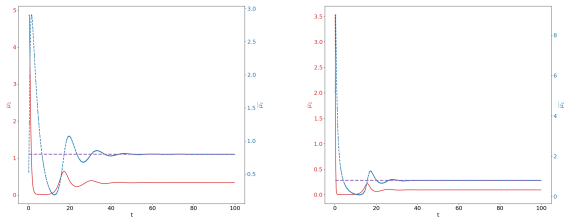

(a) $A_\sigma = 0.0001$ (b) $A_\sigma = 0.1$

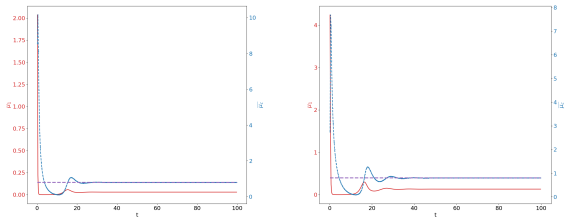

(c) $A_\sigma = 10$ (d) $A_\sigma = 100$

Figure 10: Non saturated interactions, homogeneous source of immune cells. Evolution of the tumor mass μ_1 (red curves, left axis), and of $\bar{\mu}_c$ (blue curve, right axis) for several values of A_σ.

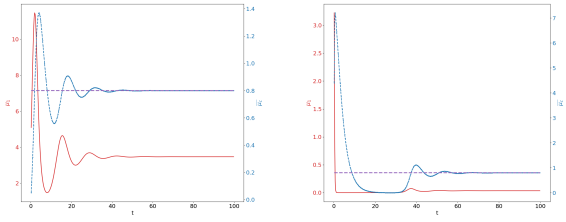

(a) $A = 0.0001$ (b) $A = 0.1$

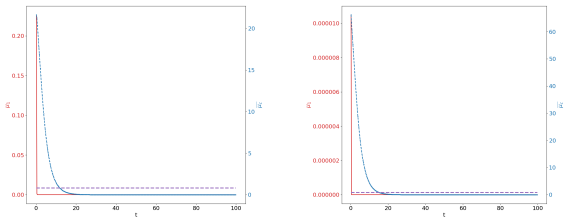

(c) $A = 10$ (d) $A = 100$

Figure 9: Non saturated interactions, homogeneous source of immune cells. Evolution of the tumor mass μ_1 (red curves, left axis), and of $\bar{\mu}_c$ (blue curve, right axis) for several values of A

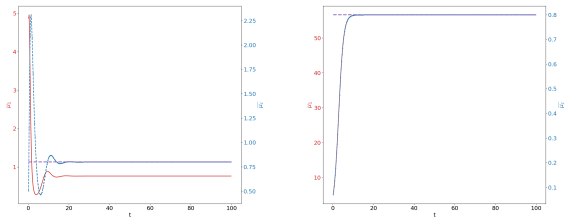

(a) $D = 0.0001$ (b) $D = 0.1$

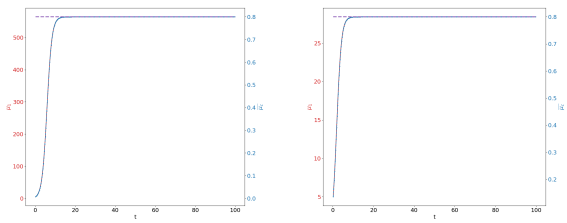

(c) $D = 10$ (d) $D = 100$

Figure 11: Non saturated interactions, homogeneous source of immune cells. Evolution of the tumor mass μ_1 (red curves, left axis), and of $\bar{\mu}_c$ (blue curve, right axis) for several values of the diffusion coefficient D.

activated T-cells are retained in the draining lymph nodes where they are activated by the dendritic cells presenting the tumor antigens and they proliferate. Once activated they migrate from the lymph nodes towards the tumor site. However, space-inhomogeneities of the source S dramatically impacts the dynamics: in many situations, with the same data as in homogeneous case but the source[1], we observe an oscillatory behavior and there is no sensitive damping at all, at least on the time scale of observation. This observation should be considered with caution (it is not excluded that the control occurs on a very long time scale and that the damping is so weak that it cannot be observed on the time scale of the simulation), bearing in mind both its mathematical signification and its practical relevance. In particular, there are cases where the asymptotic profile does not establish. In fact, what we observe is a control of a different nature: the tumor mass does not blow up, nor stabilize; instead it seems to oscillate, alternating spikes and remissions. Fig. 13 shows the

[1] the comparison makes sense since the source has in the two cases the same total mass $\int S\,\mathrm{d}x$.

space-repartition of the cytotoxic effector cells: we clearly observe the reproduction of patterns, where the concentration of active immune cells is always higher in the source sites, but can be significantly weak at the center of the domain, where the tumor stands. Meanwhile, see Fig. 14-(c) and (d), we observe a rapid growth of the tumor mass, which next shrinks significantly under the action of the immune system and then remains in a dormant state for a while, as time evolves, see [1, 10, 38] for comments on such oscillations. It is remarkable that these oscillations result only from space heterogeneities, while the model does not take into account anti-immune reactions or inflammatory mechanisms. The relevance of such oscillatory behavior has been pointed out in several modeling works, see for instance [37], where they are reproduced by introducing delays in ODEs [7, 16], or stochastic effects [8]; here they naturally emerge in the dynamic of the PDEs system.

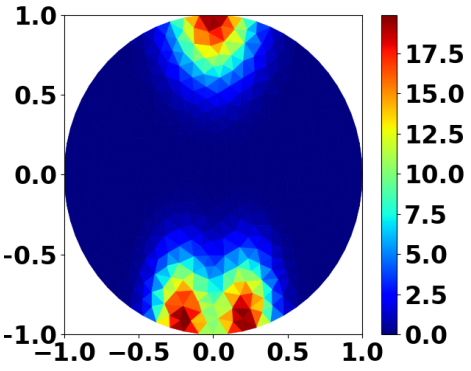

Figure 12: Heterogeneous source of immune cells S (the axis correspond to the space coordinates)

- *Tumor aggressiveness.* There is no indication, on the time of simulation of trend to an equilibrium when the division rate is large. Reducing the division rate a restores the damping, see Fig. 14, which agrees with the guess from Section 2.4.1. For larger a we observe peaks of tumor mass and immune cells, which appear regularly. The period (about 27 time units) of the oscillations does not change substantially with a. The tumor mass reaches also higher values as a increases.

  We make the immune cell death rate γ vary, for a relatively small value of a (given in Table 1). As γ increases, the equilibrium is reached faster, with less oscillations but it leads to an asymptotic state with a larger tumor mass, see Fig. 15.

- *Efficiency of the immune response.* Strengthening the immune response A or the conversion rate p damps the tumor growth, and reduces the oscillations, see Fig. 16. On the figure, we observe the delay of the immune system compared to the tumor growth. Influence of the chemoattractant effect is stronger than in the homogeneous case: increasing A_σ improves significantly the damping, see Fig. 17.

  What is remarkable is the fact that the equilibrium phase can be recovered by strengthening the chemoattractant effect: this is illustrated in Fig. 18, where the data are the same as in Fig. 14-(c), but the chemotactic strength χ has been increased.

4. Conclusive discussion

We have set up a new model intended to describe the interaction between the immune system and tumors. Based on size and space structured densities, the system of PDEs is able to take into account the displacement of tumor antigen-specific cytotoxic immune cells and the size variation of the tumor cells. Despite its simplicity the model allows us to bring out some relevant observations.

In particular, it is able to reproduce the formation of equilibrium phases, characterizing the ability of the immune system to restrain cancer growth for extended time periods. This effect, which leads to persistent tumors at a controlled level, was inferred from clinical observations and demonstrations using mouse models [19, 38]. Here, it is predicted mathematically and it has been checked numerically. This observation has important practical consequences. For instance, it is possible that this dormant state is constituted of tumors with size below the measurement capacities of the current imaging methods. However, a change in the tumor environment such as a modification of the immune system efficiency can break the control over the tumor. This is in agreement with reports on transplantation of undetected cancer from organ donor into immunosuppressed recipients [38]. Maintaining cancer in a viable equilibrium state represents a relevant goal of cancer immunotherapy. It is therefore important to understand the parameters that govern the efficiency of the immune response and the parameters to target to improve tumor control.

Moreover, the numerical experiments also show the crucial role of space organization and reveal phenomena that cannot be captured by non spatially structured models. In particular controlling the tumor with a low total mass is much more difficult when the source of immune cells is non homogeneously distributed. In such a situation, periodic patterns can be observed with the chronic formation of tumors having a significantly high mass, alternating with remission periods. Having a homogeneous source of immune cells in the peripheral environment of the tumor makes the immune response much more efficient, since it promotes an immediate contact between the tumor and the cytotoxic effector cells. Otherwise, the capacity in draining the activated immune cells towards the tumor, expressed through the strength of the chemotaxis potential, is a critical parameter of the immune response. Biologically, the role of the spatial distribution of the source of immune cells can be related to the types of cytotoxic cells considered in the modeling. The source of NK cells could be assumed to be homogenously distributed at the early stage of tumor growth. In contrast, T-cells need an efficient priming which occurs in the draining lymph nodes, and their sources is therefore

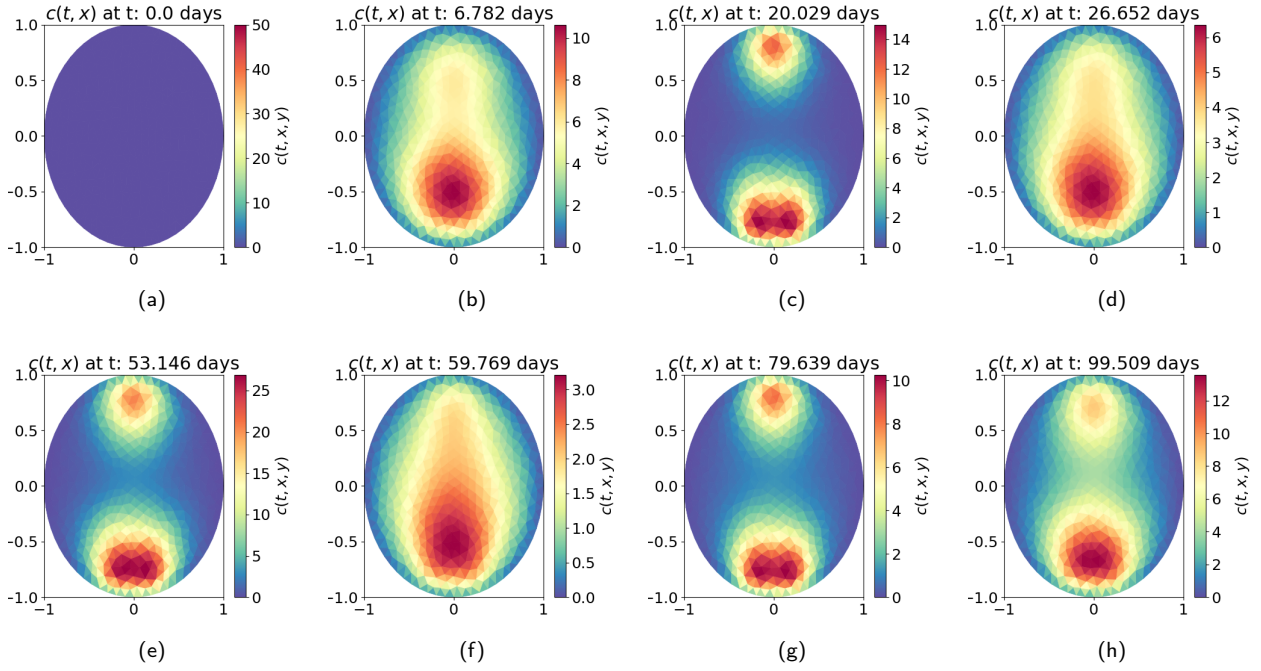

Figure 13: Time evolution of the cytotoxic effector cells concentration $c(t, x)$ (the axis correspond to the space coordinates)

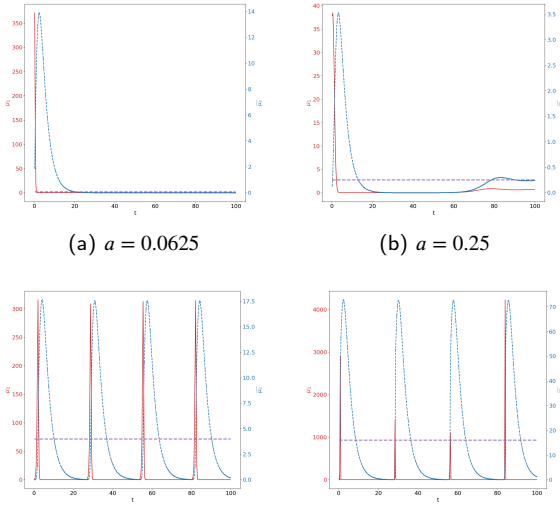

(a) $a = 0.0625$ (b) $a = 0.25$ (c) $a = 4$ (d) $a = 16$

Figure 14: Non saturated interactions, heterogeneous source of immune cells. Evolution of the tumor mass μ_1 (red curves, left axis), and of $\bar{\mu}_c$ (blue curve, right axis) for several values of the division rate a.

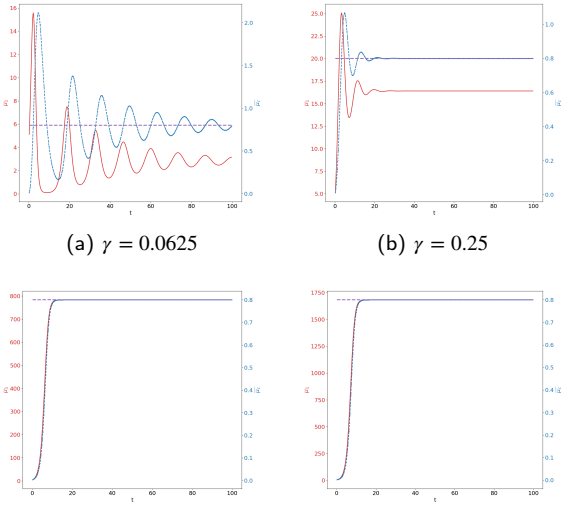

(a) $\gamma = 0.0625$ (b) $\gamma = 0.25$ (c) $\gamma = 1$ (d) $\gamma = 16$

Figure 15: Non saturated interactions, heterogeneous source of immune cells. Evolution of the tumor mass μ_1 (red curves, left axis), and of $\bar{\mu}_c$ (blue curve, right axis) for several values of the immune cells death rate γ

non-homogeneously distributed. Hence, as shown in [23], both NK and $CD8^+$ T-cells cooperate to the anti-tumor immune response and our results can illustrate the complimentary role of NK and $CD8^+$ T-cells. Moreover, our study shows that enhancing the chemoattractant effects is crucial in the immune response. Promoting the migration of T-cells towards the tumor microenvironment has indeed been identified as a possible strategy for immunotherapy [53], for instance by increasing the level of T_H1 chemokines like CXCL9 and CXCL10, which increases the level of tumor-infiltrating $CD8^+$ T cells [45]. Our findings are equally consistent with current experimental and clinical data which show the role of immune check-point in immunosuppressing T-cell responses. Indeed, T-cells express PD-1 after being activated as a mech-

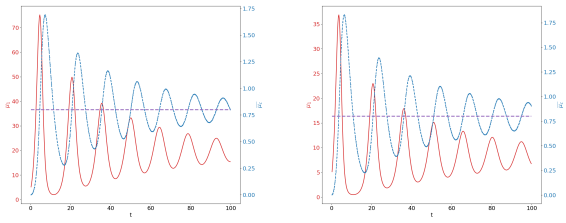

(a) $A = 0.0001$ (b) $A = 0.1$

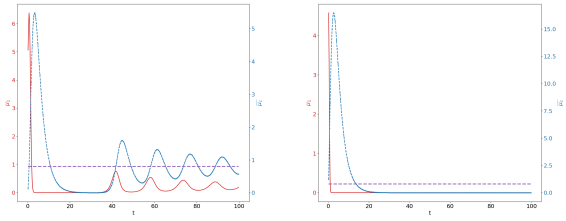

(c) $A = 10$ (d) $A = 100$

Figure 16: Non saturated interactions, heterogeneous source of immune cells. Evolution of the tumor mass μ_1 (red curves, left axis), and of $\bar{\mu}_c$ (blue curve, right axis) for several values of A

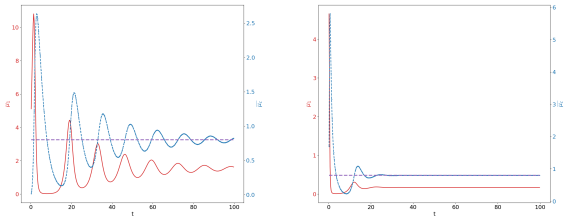

(a) $A_\sigma = 0.0001$ (b) $A_\sigma = 0.1$

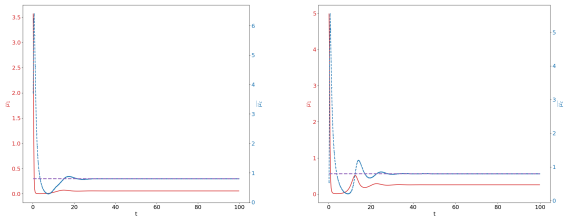

(c) $A_\sigma = 10$ (d) $A_\sigma = 100$

Figure 17: Non saturated interactions, heterogeneous source of immune cells. Evolution of the tumor mass μ_1 (red curves, left axis), and of $\bar{\mu}_c$ (blue curve, right axis) for several values of A_σ

anism of retro-control; using anti-PD-1 antibodies restores the activation of these cells (cytotoxicity and secretion of IFN-γ). A greater clearance of tumors has been observed when anti-PD-1 therapy is combined with anti-CTLA4 therapy, possibly because of the removal of a checkpoint for T-cell proliferation and priming [10]. These effects appear in the model by playing with the parameters p or A so that the immune cells are more activated or more efficient at killing tumors.

The current version of the model however misses several phenomena, which require further modeling efforts. In particular, it does not address numerous immunosuppressive mechanisms that establish as the tumor grows. For instance, in well-developed tumors, stromal activity can develop signaling modalities which inhibit T-cell activity and favor the recruitment of myeloid-derived suppressors cells, which have T-cell suppressive capacity. These effects contribute to the chronic development of tumors; they will be investigated in a forthcoming work.

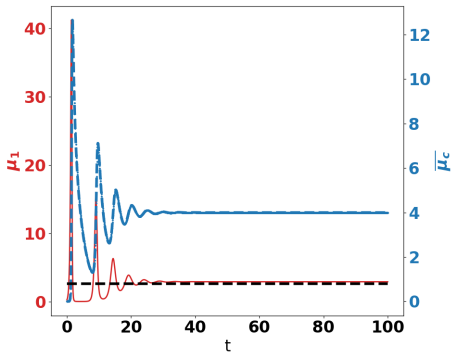

Figure 18: Non saturated interactions, heterogeneous source of immune cells. Evolution of the tumor mass μ_1 (red curves, left axis), and of $\bar{\mu}_c$ (blue curve, right axis) with $a = 4$ and $\chi = 100$

A. Tumor growth

The growth rate $z \mapsto V(z)$ can incorporate some mechanisms describing that the growth becomes more difficult for larger tumors. Relevant examples, depicted in Fig. 19, are:

- Exponential law: $V(z) = V_0 \exp(-\tau z)$ where τ is a relaxation parameter,
- Logistic law: $V(z) = V_0 \left(\dfrac{\exp(-(z-s))}{1+\exp(-(z-s))} \right)$,
- Gompertz' law: $V(z) = V_0 \exp(-b(\exp(cz)))$.

Further examples and details on the modeling of the growth rate can be found in the review [56].

In order to establish the existence of a leading eigenelement, as discussed in Section 2.4.2, the following assumptions should be fulfilled [18]:

- $\int |z'|^2 k(z'|z)\,\mathrm{d}z' < z^2$;
- $a \in L^1_{\mathrm{loc}}((0,\infty)) \cap \mathcal{F}$, where $\mathcal{F}$ is the set of non negative functions f such that we can find $p, q \geq 0$ verifying $\limsup_{z\to\infty} z^{-p} f(z) < \infty$ and $\liminf_{z\to\infty} z^{q} f(z) > 0$;
- there exists $r \geq 0$ such that $\mathrm{supp}(a) \subset [r, \infty)$;
- there exists $\alpha_1 \geq 0$ such that $z^{\alpha_1} V(z) \in L^\infty_{\mathrm{loc}}$ and for any compact $K \subset (0,\infty)$ we can find $c_K > 0$ such that $V(z) \geq c_K$ a.e. on K;

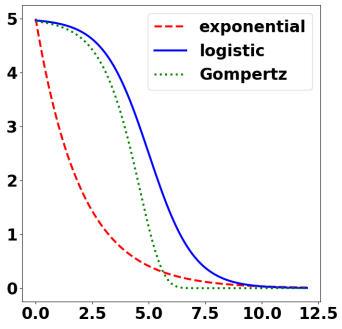

Figure 19: Shape of several growth laws $z \mapsto V(z)$ (x-axis: z, size of the tumor cells, y-axis: growth rate of the cells)

- for a certain $\gamma \geq 0$, $z \mapsto \frac{z^\gamma}{V(z)}$ lies in the set L^1_0 of functions f for which there exists $d > 0$ such that $f \in L^1((0,d))$;
- there exists $M \geq 0, \gamma \geq 0$ such that $\int_0^s k(z'|z)\,\mathrm{d}z' \leq \min(1, M(s/z)^\gamma)$;
- $\frac{a}{V}$ also lies in L^1_0 and it verifies $\lim_{z\to\infty} \frac{za(z)}{V(z)} = \infty$.

We refer the reader to [18] for further comments and interpretations on the these assumptions, which guaranty existence-uniqueness for (26).

B. Model parameters

Table 2 collects the information about variables, parameters and units for the tumor growth model, and Table 3 details the units of the parameters of the equations for the immune system.

Remark 3. *The model can take into account two distinct saturation effects: the former in the expression of the recruitment term of the cytotoxic effector cells, through the function g, the latter in the expression of the death term describing the action of the activated immune cells on the tumor. We also work with saturationless models, which means*

$$g(\mu_1) = \mu_1, \qquad m(c,n) = n\int_\Omega \delta(y)c(t,y)\,\mathrm{d}y.$$

We leave the reader adapt the definition of the units to such cases.

C. Numerical method

For the numerical simulation of the model, we use the so-called finite volume approach, for which we refer the reader to [22].

The growth-division equation. The computational domain for the size variable is the interval $[0, z_\star]$ where $z_\star$ is chosen large enough: due to the division processes, we expect the the solution remains essentially on a bounded interval, and the cut-off should not perturb too much the solution. For the simplified binary division model, a guess is provided by using the profile given by Lemma 1. This domain is split into cells $M_i = (z_{i-1/2}, z_{i+1/2})$, centered on $z_i = \frac{z_{i-1/2}+z_{i+1/2}}{2}$ where $z_0 = z_{1/2} = 0 < \ldots < z_{i-1/2} < z_i < z_{i+1/2} < \ldots < z_{N+1/2} = z_{N+1} = z_\star$. In what follows, the step $\Delta z = z_{i+1/2} - z_{i-1/2}$ is assumed to be constant. We denote by Δt the time step and $t^\kappa = \kappa\Delta t$. The discrete unknowns n_i^κ, with $i \in \{1,\ldots,I\}$ and $\kappa \in \{1,\ldots,N_t\}$ are intended to be approximation of the mean value $\frac{1}{\Delta z}\int_{M_i} n(t^\kappa, z)\,\mathrm{d}z$. The integral that defines the gain term of the division operator is approximated by a simple quadrature rule. For the operator (11) the kernel involves Dirac masses which are approached by peaked Gaussian. The scheme reads

$$\begin{aligned}\Delta z\frac{n_i^{\kappa+1}-n_i^\kappa}{\Delta t} + F^\kappa_{i+1/2} - F^\kappa_{i-1/2} \\ = -a_i\Delta z n_i^\kappa + \Delta z^2\sum_{j=1}^{I} a(z_j)k(z_i|z_j)n_j^\kappa - m_i^\kappa,\end{aligned} \tag{31}$$

where $F^\kappa_{i+1/2} = V_{i+1/2}n_i^\kappa$ represents the convective numerical flux on the interfaces of $z_{i+1/2}$, which is defined according to the upwinding principle and m_i^κ is the approximation of the interaction term (see below). Note that the step Δz should be small enough to capture the division of small cells, if any.

We can use formula (1) to check that the numerical procedure preserves the eigen-function of the growth division equation when m is replaced by 0 and using the eigen-function as initial data.

The effector cytotoxic cells displacement equation. We work with a tessellation of Ω made of triangles, that form an admissible mesh of Ω, see [22, Definition 3.1, sp. (iv)]. Let K be a control volume of the mesh τ_Ω. The set of the edges of the mesh is noted ξ. We distinguish the edges on $\partial\Omega$ and the internal edges: $\xi = \xi^{\mathrm{ext}} \cup \xi^{\mathrm{int}}$. We also denote $\xi_K = \{\varsigma \in \xi \cap \partial K\}$, $d_{K\varsigma}$ the distance from the point x_K to the edge ς and $|K|$ stands for the two dimensional measure of the control volume K, $|\varsigma|$ for the length of an edge $\varsigma \in \xi$. If $\varsigma \in \xi^{\mathrm{int}}$, then $\varsigma = K|L$ and the distance d_{KL} between x_K and x_L is equal to $d_{K\varsigma} + d_{L\varsigma}$.

The chemotactic convection can be very strong and impact severely the stability condition of a scheme that would be explicit on the transport part of the equation. For this reason, we use an implicit approach defined by

$$\begin{aligned}|K|\frac{c_K^{\kappa+1}-c_K^k}{\Delta t} \\ = \left(-\sum_{\varsigma\in\xi_K}\mathcal{F}_{K\varsigma}(c^{\kappa+1}_{\tau_\Omega}, \phi^\kappa_{\tau_\Omega}) - \sum_{\varsigma\in\xi_K}\mathcal{G}_{K\varsigma}(D, c^{\kappa+1}_{\tau_\Omega})\right) \\ +|K|p\mu_1^\kappa S_K - |K|\gamma c_K^{\kappa+1},\end{aligned} \tag{32}$$

and then we update the chemotactic potential by

$$-\sum_{\varsigma\in\xi_K}\mathcal{G}_{K\varsigma}(\mathcal{K}, \phi^{\kappa+1}_{\tau_\Omega}) = |K|\mu_1\langle\sigma\rangle_K. \tag{33}$$

variables	descriptions	units	example of units	Estimated values examples	Source
z	volume of tumor cells	$[l]^3$	μm^3	$\sim 10^3 \mu m^3$ (in average)	
t	time variable	$[t]$	day		
n	density of tumor cells with a volume z	$[cell_n] \cdot [l]^3$	$cell_n \cdot \mu m^{-3}$	A tumor reaching the size of $1cm^3$ (approximately $1g$ wet weight) is commonly assumed to contain 1×10^9cells ($10^{-3} cell_n \cdot \mu m^{-3}$)	[13]
V	tumor cells growth rate	$[l]^3 \cdot [t]$	$\mu m^3 \cdot day^{-1}$	$0.985 \cdot 10^3 \mu m^3 \cdot day^{-1}$ (Breast tumor)	
a	rate at which a cell of size z divides	$[l]^{-1}$	day^{-1}		
k	distribution of cells from a cell of size z dividing	$[l]^{-3}$	μm^{-1}		
μ_0	total number of tumor cells in the tumor	$[cell_n]$	$cell_n$		
μ_1	total volume of the tumor	$[cell_n] \cdot [l]^3$	$cell_n \cdot \mu m^3$		

Table 2
Recap of the main definitions and notations for the tumor growth model

variables	descriptions	units	example of units	Estimated values examples	Source
x	space variable	$[L]$	mm		
c	concentration of activated cytotoxic effector cells	$[cell_c] \cdot [L]^{-3}$	$cell_c \cdot mm^{-3}$		
χ	chemotactic coefficient	$[L]^2 \cdot [t]^{-1} \cdot [mol]^{-1}$	$mm^2 \cdot mmol^{-1} \cdot day^{-1}$	$10^{-2} - 10^3 cm^2 s^{-1} mol^{-1}$ or $8.64 \times 10^1 - 8.64 \times 10^6 mm^2 \cdot mmol^{-1} \cdot day^{-1}$ (Macrophages)	Farell and al. 1990 [25]
ϕ	attractive potential	$[mol]$	$mmol$		
D	natural space diffusion coef. of the cytotoxic effector cells population	$[L]^2 \cdot [t]^{-1}$	$mm^2 \cdot day^{-1}$	$8.64 \times 10^{-7} cm^2 \cdot s^{-1}$ or $8.64 \times 10^{-5} mm^2 \cdot day^{-1}$ (cytotoxic effector cells) (or $0.025 mm^2 \cdot day^{-1}$ for effector T-cells)	A. Friedman et al. [26], (A.K. Cooper et al. [11])
p	conversion rate of immune cell into tumor antigen-specific cytotoxic effector cells	$[t]^{-1}$	day^{-1}	$0.25 \quad day^{-1}$ (IL-2 induced activation)	A. Friedman et al. [26]
S	density of the source of immune cells	$[cell_c] \cdot [L]^{-3}$	$cell_c \cdot mm^{-3}$		
β	steepness coefficient of the immune cell recruitment	$[cell_n]$	$cell_n$		
γ	natural death rate of the tumor antigen-specific cytotoxic effector cells	$[t]^{-1}$	day^{-1}	$0.18 \quad day^{-1}$	A. Friedman et al. [26]
$\mathcal{K}$	natural space diffusion of the attractive potential ϕ	$[L]^2 \cdot [t]^{-1}$	$mm^2 \cdot day^{-1}$	$2.16 \ mm^2 \cdot day^{-1}$	
σ	chemical signal induced by each tumor cell	$[mol] \cdot n^{-1} \cdot [l]^{-3} [t]^{-1}$	$mmol \cdot cell_n^{-1} \cdot \mu m^{-3} \cdot day^{-1}$	$200 \cdot 10^{-3} \ mmol \cdot -_A^{-1} \cdot day^{-1}$	
δ	strength of the immune response	$\frac{[cell_n]}{[cell_c] \cdot [t] \cdot [l]^3}$	$cell_n \cdot cell_c^{-1} \cdot \mu m^{-3} \cdot day^{-1}$	$1 \quad day^{-1}$, average rate at which effector T-cells kill tumor cells	A. K. Cooper et al. [11]
α	steepness coefficient of the tumor cell death term	$[cell_n] \cdot [l]^3$	$cell_n \cdot \mu m^{-3}$		

Table 3
Recap of the main definitions and notations for the immune system model

In (32)-(33), we have used the following notations:

- for the diffusive flux of a quantity w, with the diffusion matrix A, we set

$$\mathcal{G}_{K\varsigma}(A, w_{\tau_\Omega}) = A_\varsigma \frac{|\varsigma|}{d_{KL}}(w_K - w_L) \quad \text{if } \varsigma \in \xi^{\text{int}}$$

with the necessary adaptation on the boundary, according to the boundary condition (Dirichlet or Neumann),

- for the convective flux, we set

$$\mathcal{F}_{K\varsigma}(c_{\tau_\Omega}, \phi_{\tau_\Omega}) = \frac{|\varsigma|}{d_{KL}}\left(\chi c_K(\phi_L - \phi_K)^+ - \chi c_L(\phi_L - \phi_K)^-\right) \quad \text{for } \varsigma \in \xi^{\text{int}},$$

and $\mathcal{F}_{K\varsigma}(c_{\tau_\Omega}, \phi_{\tau_\Omega}) = 0$ if $\varsigma \in \xi^{\text{ext}}$.

The expression of the interaction term in (31) depends on the details on the death term; for instance when it depends linearly on c and n, it reads

$$m_i^\kappa = n_i^\kappa \sum_{K\in\tau_\Omega} |K|\delta_K c_K^\kappa.$$

The time step Δt is determined in order to preserve the positivity of the solution, namely we assume the following CFL stability condition:

$$\Delta t \leq \min\left(\frac{\Delta z}{\max_{0\leq z\leq z_\star} V(z)}, \frac{1}{\max_{0\leq z\leq z_\star} a(z)}, \frac{1}{\sum_{K\in\tau_\Omega} |K|\delta_K c_K^\kappa}\right).$$

D. Supplementary material

D.1. Non-saturated interactions and saturated conversion of effector cells

In this Section, we discuss the saturation effect taken into account in the conversion from non activated immune cells to effector cytotoxic cells. Namely, in the evolution equation for c, we take $\mu_1 \mapsto g(\mu_1)$ as in (12), with $\beta = 5000$. The other parameters are still as in Table 1. The saturation effect accounts for the fact that the activation process of immune cells is limited. We can expect that as the threshold decreases, the immune system is less efficient in controlling the tumor growth.

On the simulations, we still observe the asymptotic trend towards an equilibrium, as predicted by the theoretical results. However, the tumor mass is considerably higher than for the saturation-free model, see Fig. 20. With an homogeneous source of immune cells, the control still occurs as the death rate γ of the cytotoxic effector cells increases, but the high asymptotic tumor mass reveals a loss of efficiency of the immune system, see Fig. 21. When the source of immune cells is heterogeneous (we work with the same distribution as in Fig. 12), the control is lost as γ increases, see Fig. 22. The saturation effect can be discussed also by making the steepness parameter β vary. As β is reduced, the control is not lost, but the asymptotic mass of the tumor becomes higher, see Fig. 23 and 24.

D.2. Saturated interactions and non-saturated conversion of effector cells

In this section, let us briefly discuss the saturation effect taken into account in the interaction between the effector cells and the tumor cells. Namely, in the tumor growth

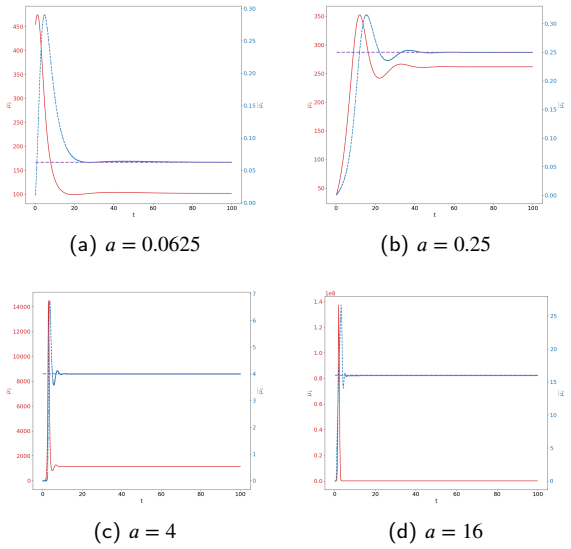

(a) $a = 0.0625$ (b) $a = 0.25$ (c) $a = 4$ (d) $a = 16$

Figure 20: Saturated conversion, homogeneous source of immune cells. Evolution of the tumor mass μ_1 (red curves, left axis), and of $\bar{\mu}_c$ (blue curve, right axis) for several values of a.

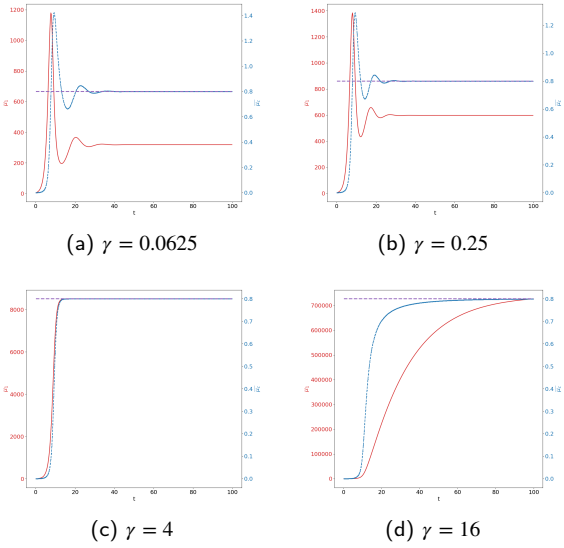

(a) $\gamma = 0.0625$ (b) $\gamma = 0.25$ (c) $\gamma = 4$ (d) $\gamma = 16$

Figure 21: Saturated conversion, homogeneous source of immune cells. Evolution of the tumor mass μ_1 (red curves, left axis), and of $\bar{\mu}_c$ (blue curve, right axis) for several values of γ.

equation, the interaction term becomes

$$m(c,n)(t,z) = \int_\Omega \delta(y)c(t,y)\,\mathrm{d}y \times \frac{n(t,z)}{\alpha + n(t,z)},$$

as in (21), with $\alpha\alpha' = 1$. For the numerical tests, we set $\alpha = 3000$. The other parameters are as in Table 1. This expression traduces the fact that the tumor antigen-specific cytotoxic effector cells have access to a limited amount of tumor cells. We point out that our analysis by means of eigen-elements does not apply here since we have introduced

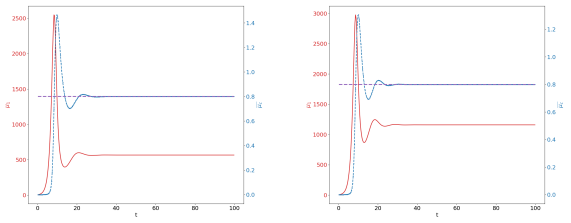

(a) $\gamma = 0.0625$ (b) $\gamma = 0.25$

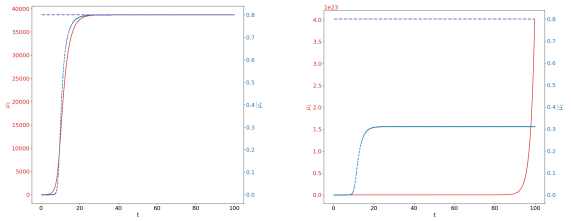

(c) $\gamma = 4$ (d) $\gamma = 16$

Figure 22: Saturated conversion, heterogeneous source of immune cells. Evolution of the tumor mass μ_1 (red curves, left axis), and of $\bar{\mu}_c$ (blue curve, right axis) for several values of γ.

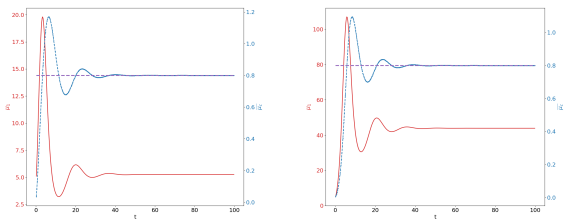

(a) $\beta = 10$ (b) $\beta = 100$

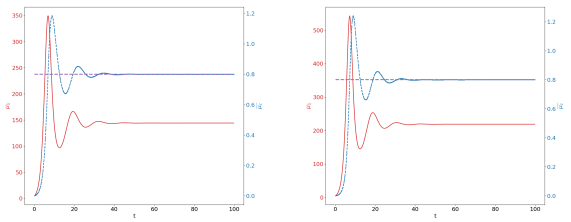

(c) $\beta = 500$ (d) $\beta = 1000$

Figure 23: Saturated conversion, homogeneous source of immune cells. Evolution of the tumor mass μ_1 (red curves, left axis), and of $\bar{\mu}_c$ (blue curve, right axis) for several values of β.

non linearities with respect to n in the tumor growth equation. Nevertheless, we can investigate on numerical grounds whether or not the immune system can control the tumor growth in this case.

We observe, see Fig. 25 (homogeneous source of immune cells), an effective control of the tumor evolution, at least when the tumor is not too agressive, with a moderate division rate a. When a becomes larger, the tumor mass grows exponentially fast. Similar features are observed with a non homogeneous source of immune cells.

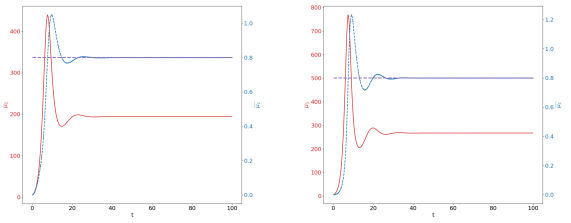

(a) $\beta = 10$ (b) $\beta = 100$

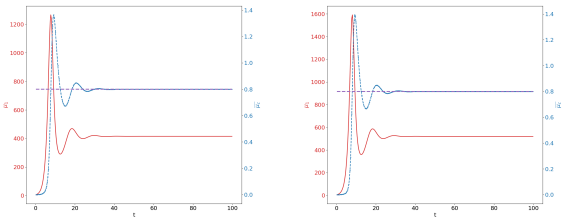

(c) $\beta = 500$ (d) $\beta = 1000$

Figure 24: Saturated conversion, heterogeneous source of immune cells. Evolution of the tumor mass μ_1 (red curves, left axis), and of $\bar{\mu}_c$ (blue curve, right axis) for several values of β.

As we make α vary, we observe two phenomena: when α increases, both the frequency of oscillations is higher and the damping is stronger, see Fig. 26 (homogeneous source of immune cells). We get a similar behavior by playing with A_σ. Surprisingly, with an heterogeneous source of immune cells, the periodic behavior observed in the saturation-less case reappears when α (or A_σ) is small, see Fig. 27. (In Fig. 27-(a) the behavior is also periodic but the period is higher than the represented simulation time.)

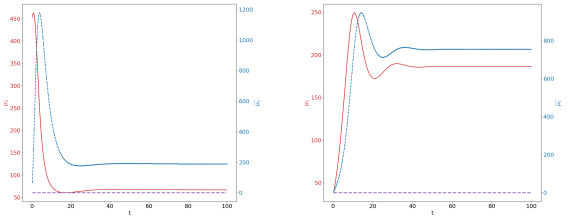

(a) $a = 0.0625$ (b) $a = 0.25$

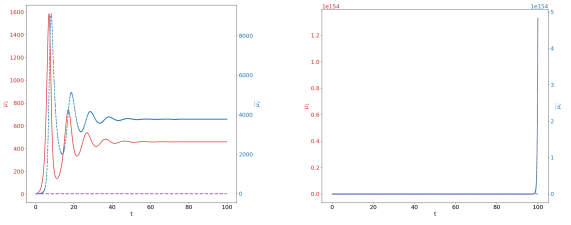

(c) $a = 1$ (d) $a = 4$

Figure 25: Saturated interactions, homogeneous source of immune cells. Evolution of the tumor mass μ_1 (red curves, left axis), and of $\bar{\mu}_c$ (blue curve, right axis) for several values of a.

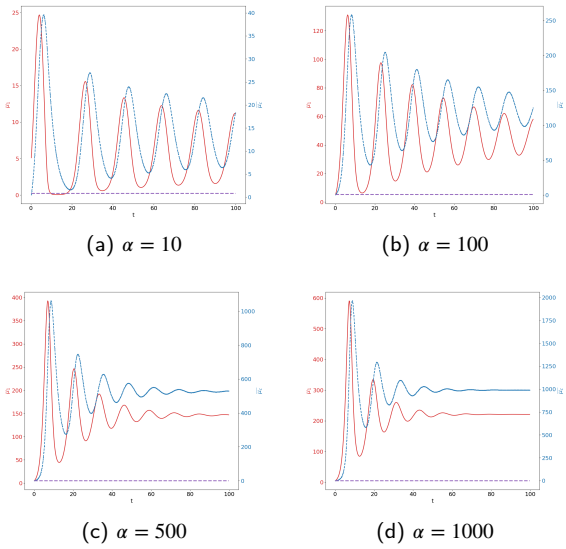

(a) $\alpha = 10$ (b) $\alpha = 100$

(c) $\alpha = 500$ (d) $\alpha = 1000$

Figure 26: Saturated interactions, homogeneous source of immune cells. Evolution of the tumor mass μ_1 (red curves, left axis), and of $\bar{\mu}_c$ (blue curve, right axis) for several values of α.

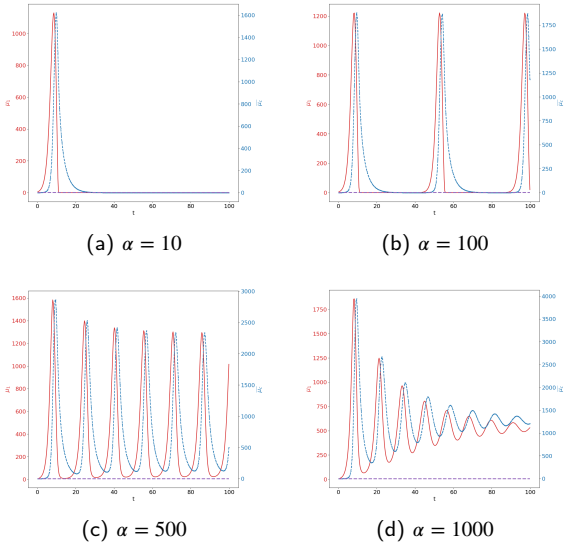

(a) $\alpha = 10$ (b) $\alpha = 100$

(c) $\alpha = 500$ (d) $\alpha = 1000$

Figure 27: Saturated interactions, heterogeneous source of immune cells. Evolution of the tumor mass μ_1 (red curves, left axis), and of $\bar{\mu}_c$ (blue curve, right axis) for several values of α.

D.3. Multiple tumor sites

The model can be adapted to consider the relevant situation where there are many tumor sites. With q the number of tumor sites, we can consider possibly different parameters governing the growth and the immune interactions. Let

- n_i be the size-structured distribution of tumor cells in the site $i \in \{1, ..., q\}$;
- V_i, a_i and δ_i be the corresponding growth rate, division rate and immune strengths, respectively;

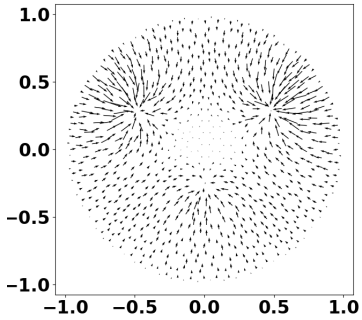

Figure 28: Chemotactic potential at $t = 0.12$ in the case of multiple tumor sites with different division rates

- σ_i be the form function describing the signal emitted by each tumor.

The model becomes

$$\begin{cases} \partial_t n_i + \partial_z(V_i n_i) = Q_i(n_i) - n_i \displaystyle\int_\Omega \delta_i(x) c(t,x)\,\mathrm{d}x, \\ \partial_t c + \nabla_x \cdot (\chi c \nabla_x \phi - D \nabla_x c) \\ \qquad = pS \displaystyle\sum_{i=1}^{q} \int_0^\infty z n_i(t,z)\,\mathrm{d}z - \gamma c, \\ -\nabla_x \cdot (\mathcal{K} \nabla_x \phi) = \displaystyle\sum_{i=1}^{q} \int_0^\infty z n_i(t,z)\,\mathrm{d}z \langle \sigma_i \rangle, \end{cases} \tag{34}$$

endowed with initial and boundary conditions. For the numerical test, we deal with $q = 3$ tumor sites, located at the positions

$$x_1 = (0, -0.30), \qquad x_2 = (0.5, 0.3), \qquad x_3 = (-0.5, 0.3).$$

We assume that the tumor sites have the same constant growth rate V, immune strength δ and form function σ, but distinct division rates, $a, 2a, 1.5a$. The parameters are defined as in Table 1. We work with the heterogeneous source of immune cells illustrated in Fig. 12. The behavior of the tumor mass and immune cells mass has the same features as in the single site case, see Fig. 29.

Acknowledgements

The authors acknowledge the support of the University Côte d'Azur research network UCAncer, which is a strong incentive for this collaboration.

References

[1] Z. Agur, K. Halevi-Tobias, Y. Kogan, and O. Shlagman. Employing dynamical computational models for personalizing cancer immunotherapy. *Expert Opinion on Biological Therapy*, 16(11):1373–1385, 2016.

[2] N. André, D. Barbolosi, F. Billy, G. Chapuisat, F. Hubert, E. Grenier, and A. Rovini. Mathematical model of cancer growth controled by metronomic chemotherapies. *ESAIM:ProcS*, 41:77–94, 2013.

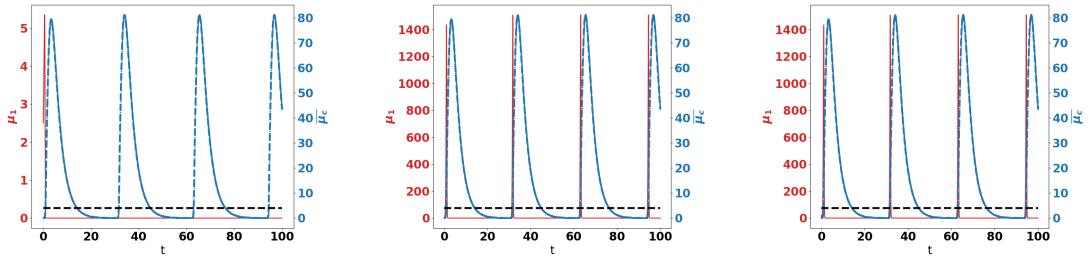

(a) a (b) $2a$ (c) $1.5a$

Figure 29: Evolution of the tumor masses μ_1 (red curves, left axis), and of $\bar{\mu}_c$ (blue curve, right axis) for three different tumor sites.

[3] K. Atsou, F. Anjuère, V. Braud, and T. Goudon. Numerical investigation of the equilibrium phase in immune-controlled tumor. Work in preparation, 2020.

[4] F. Baccelli, D.R. McDonald, and J. Reynier. A mean field model for multiple TCP connections through a buffer implementing RED. *Performance Evaluation*, 49(1-4):77–97, 2002.

[5] B. Basse, B. C. Baguley, E.S. Marshall, W. R. Joseph, B. van Brunt, G. Wake, and D. J. N. Wall. A mathematical model for analysis of the cell cycle in cell lines derived from human tumors. *J. Math. Biol.*, 47(4):295–312, 2003.

[6] F. Bekkal Brikci, J. Clairambault, B. Ribba, and B. Perthame. An age-and-cyclin-structured cell population model for healthy and tumoral tissues. *J. Math. Biol.*, 57(1):91–110, 2008.

[7] P. Bi, S. Ruan, and X. Zhang. Periodic and chaotic oscillations in a tumor and immune system interactionmodel with three delays. *Chaos*, 24:023101, 2014.

[8] G. Caravagna, A. d'Onofrio, P. Milazzo, and R. Barbuti. Tumour suppression by immune system through stochastic oscillations. *J. Theor. Biol.*, 265(3):336–345, 2010.

[9] D. A. Chen and I. Mellman. Oncology meets immunology: The cancer immunity cycle. *Immunity*, 39(1):1–10, 2013.

[10] D. A. Chen and I. Mellman. Elements of cancer immunity and the cancer-immune set point. *Nature*, 541:321–330, 2017.

[11] A. K. Cooper and P. S. Kim. A cellular automata and a partial differential equation model of tumor–immune dynamics and chemotaxis. In A. Eladdadi, P. Kim, and D. Mallet, editors, *Mathematical Models of Tumor-Immune System Dynamics*, pages 21–46, New York, NY, 2014. Springer New York.

[12] L. G. de Pillis, A. E. Radunskaya, and C. L. Wiseman. A validated mathematical model of cell-mediated immune response to tumor growth. *Cancer Res.*, 65(17):7950–7958, 2005.

[13] U. Del Monte. Does the cell number 109 still really fit one gram of tumor tissue? *Cell Cycle*, 8(3):505–506, 2009. PMID: 19176997.

[14] A. Devys, T. Goudon, and P. Lafitte. A model describing the growth and size distribution of multiple metastatic tumors. *Disc. Cont. Dyn. Syst.-B*, 12:731–767, 2009.

[15] A. d'Onofrio. A general framework for modeling tumor-immune system competition and immunotherapy: mathematical analysis and biomedical inferences. *Physica D*, 208(3-4):220–235, 2005.

[16] A. d'Onofrio, Gatti. F., P. Cerrai, and L. Fresch. Delay-induced oscillatory dynamics of tumour-immune system interaction. *Math. Comput. Model.*, 51:572–591, 2010.

[17] M. Doumic. *Growth-fragmentation equations in biology*. Habilitation à diriger des recherches, Université Pierre et Marie Curie - Paris VI, June 2013.

[18] M. Doumic-Jauffret and P. Gabriel. Eigenelements of a general aggregation-fragmentation model. *Math. Models Meth. App. Sci.*, 20(5):757–783, 2010.

[19] G. P. Dunn, A. T. Bruce, H. Ikeda, L. J. Old, and R. D. Schreiber. Cancer immunoediting: from immunosurveillance to tumor escape. *Nature Immunology*, 3:991–998, 2002.

[20] R. Eftimie, J. L. Bramson, and D. J. D. Earn. Interactions between the immune system and cancer: A brief review of non-spatial mathematical models. *Bull. Math. Biol.*, 73(1):2–32, Jan 2011.

[21] R. Eftimie, J. J. Gillard, and D. A. Cantrell. Mathematical models for immunology: Current state of the art and future research directions. *Bull. Math. Biol.*, 78:2091–2134, 2017.

[22] R. Eymard, T. Gallouët, and R. Herbin. Finite volume methods. In P. Ciarlet and J.-L. Lions, editors, *Handbook of Numerical Analysis, Vol. VII*, volume VII of *Handb. Numer. Anal.*, pages 715–1022. North-Holland, 2000.

[23] J. Faget, S. Groeneveld, G. Boivin, M. Sankar, N. Zangger, M. Garcia, N. Guex, I. Zlobec, L. Steiner, A. Piersigilli, I. Xenarios, and E. Meylan. Neutrophils and snail orchestrate the establishmentof a pro-tumor microenvironment in lung cancer. *Cell Report*, 21:3190–3204, 2017.

[24] J. D. Farrar, K. H. Katz, J. Windsor, G. Thrush, R. H. Scheuermann, J. W. Uhr, and N. E. Street. Cancer dormancy. VII. a regulatory role for $CD8+$ t-cells and $IFN-\gamma$ in establishing and maintaining the tumor-dormant state. *J. Immunol.*, 162(5):2842–2849, 1999.

[25] B. E. Farrell, R. P. Daniele, and D. A. Lauffenburger. Quantitative relationships between single-cell and cell-population model parameters for chemosensory migration responses of alveolar macrophages to C5a. *Cell Motility*, 16(4):279–293, 1990.

[26] A. Friedman and W. Hao. The role of exosomes in pancreatic cancer microenvironment. *Bull. Math. Biol.*, 80(5):1111–1133, May 2018.

[27] P. Gabriel. *Transport-fragmentation equations and applications to prion diseases*. Phd thesis, Université Pierre et Marie Curie - Paris VI, June 2011.

[28] N. Glodde, T. Bald, D. van den Boorn-Konijnenberg, K. Nakamura, J. S. O'Donnell, S. Szczepanski, M. Brandes, S. Eickhoff, I. Das, N. Shridhar, D. Hinze, M. Rogava, T. C. van der Sluis, J. J. Ruotsalainen, Gaffal. E., J. Landsberg, K. U. Ludwig, C. Wilhelm, M. Riek-Burchardt, A. J. Müller, C. Gebhardt, R. A. Scolyer, G. V. Long, V. Janzen, M. W. L. Teng, W. Kastenmüller, M. Mazzone, M. J. Smyth, T. Tüting, and M. Hölzel. Reactive neutrophil responses dependent on the receptor tyrosine kinase $c-MET$ limit cancer immunotherapy. *Immunity*, 47(4):789 – 802.e9, 2017.

[29] D. Hanahan and R. A. Weinberg. The hallmarks of cancer. *Cell*, 100:57–70, 2000.

[30] T. Hillen and K. J. Painter. A user's guide to PDE models for chemotaxis. *J. Math. Biol.*, 58(1):183, Jul 2008.

[31] D. Horstmann. From 1970 until present: the Keller-Segel model in chemotaxis and its consequences. I. *Jahresber. Deutsch. Math.-Verein.*, 105:103–165, 2003.

[32] D. Horstmann. From 1970 until present: the Keller-Segel model in chemotaxis and its consequences. II. *Jahresber. Deutsch. Math.-Verein.*, 106:51–69, 2003.

[33] E. Itakura, R.-R. Huang, D.-R. Wen, E. Paul, P. H. Wünsch, and A. J.

Cochran. IL-10 expression by primary tumor cells correlates with melanoma progression from radial to vertical growth phase and development of metastatic competence. *Mod. Pathol.*, 24(6):801–809, 2011.

[34] Y. Iwai, M. Ishida, Y. Tanaka, T. Okazaki, T. Honjo, and N. Minato. Involvement of PD-L1 on tumor cells in the escape from host immune system and tumorimmunotherapy by PD-L1 blockade. *Proc. Natl. Acad. Sci.*, 99(19):12293–12297, 2002.

[35] J. N. Kather, J. Poleszczuk, M. Suarez-Carmona, J. Krisam, P. Charoentong, N. A. Valous, C.-A. Weis, L. Tavernar, F. Leiss, E. Herpel, F . Klupp, A. Ulrich, M. Schneider, A. Marx, D. Jäger, and N. Halama. *In Silico* modeling of immunotherapy and stroma-targeting therapies in human colorectal cancer. *Cancer Res.*, 77(22):6442–6452, 2017.

[36] E. F. Keller and L. A. Segel. Model for chemotaxis. *J. Theor. Biol.*, 30(2):225 – 234, 1971.

[37] D. Kirschner and J. C. Panetta. Modeling immunotherapy of the tumor-immune interaction. *J. Math. Biol.*, 37:235–252, 1998.

[38] C. M. Koebel, W. Vermi, J. B. Swann, N. Zerafa, S. J. Rodig, L. J. Old, M. J. Smyth, and R. D. Schreiber. Adaptive immunity maintains occult cancer in an equilibrium state. *Nature*, 450:903–908, 2007.

[39] V. A. Kuznetsov, I. A. Makalkin, M. A. Taylor, and A. S. Perelson. Nonlinear dynamics of immunogenic tumors: Parameter estimation and global bifurcation analysis. *Bull. Math. Biol.*, 56(2):295–321, Mar 1994.

[40] A. Matzavinos, M. A. J. Chaplain, and V. A. Kuznetsov. Mathematical modelling of the spatio-temporal response of cytotoxic T-lymphocytes to a solid tumour. *Mathematical Medicine and Biology*, 21(1):1–34, 2004.

[41] E. D. McGrady and Robert M. Ziff. "Shattering" transition in fragmentation. *Phys. Rev. Lett.*, 58:892–895, Mar 1987.

[42] P. Michel. Existence of a solution to the cell division eigenproblem. *Math. Models Meth. App. Sci.*, 16(Suppl. issue 1):1125–1153, 2006.

[43] P. Michel, S. Mischler, and B. Perthame. General relative entropy inequality: an illustration on growth models. *J. Math. Pures et Appl.*, 84(9):1235–1260, 2005.

[44] M. Müller, F. Gounari, S. Prifti, H. J. Hacker, V. Schirrmacher, and K. Khazaie. Eblacz tumor dormancy in bone marrow and lymph nodes: Active control of proliferating tumor cells by $CD8+$ immune T-cells. *Cancer Research*, 58(23):5439–5446, 1998.

[45] N. Nagarsteth, M. S. Wicha, and W. Zou. Chemokines in the cancer microenvironment and their relevance in cancer immunotherapy. *Nat. Rev. Immunol.*, 17:559–572, 2017.

[46] S. Olver, P . Groves, K. Buttigieg, E. S. Morris, M. L. Janas, A. Kelso, and N. Kienzle. Tumor-derived Interleukin-4 reduces tumor clearance and deviates the cytokine and granzyme profile of tumor-induced $CD8^+$ T-cells. *Cancer Res.*, 66(1):571–580, 2009.

[47] B. Perthame. *Transport equations in biology*. Frontiers in Math. Birkhauser, 2007.

[48] B. Perthame and L. Ryzhik. Exponential decay for the fragmentation or cell-division equation. *J. Differential Equations*, 210:155–177, 2005.

[49] G. A. Rabinovich, D. Gabrilovich, and E. M. Sotomayor. Immunosuppressive strategies that are mediated by tumor cells. *Ann. Rev. Immunol.*, 25(1):267–296, 2007. PMID: 17134371.

[50] M. Robertson-Tessi, A. El-Kareh, and A. Goriely. A mathematical model of tumor–immune interactions. *J. Theor. Biol.*, 294:56 – 73, 2012.

[51] H. Salmon, K. Franciszkiewicz, D. Damotte, P. Validire, A. Trautmann, F. Mami-Chouaib, and E. Donnadieu. Matrix architecture defines the preferential localization and migration of T-cells into the stroma of human lung tumors. *J. Clinical Investigation*, 122(3):899–910, 2012.

[52] J. Shimizu, S. Yamazaki, and S. Sakaguchi. Induction of tumor immunity by removing $CD25^+$ $CD4^+$ t-cells: A common basis between tumor immunity and autoimmunity. *J. Immunol.*, 163:5211–5218, 1999.

[53] C. Y. Slaney, M. H. Kershaw, and P. K. Darcy. Trafficking of t-cells into tumors. *Cancer Res.*, 74:7168–7174, 2014.

[54] M. J. Smyth, D. I. Godfrey, and J. A. Trapani. A fresh look at tumor immunosurveillance and immunotherapy. *Nat. Immunol.*, 2, 2001.

[55] T. H. Stewart. Immune mechanisms and tumor dormancy. *Medicina (B Aires)*, 56(Suppl. 1):74–82, 1996.

[56] A. Talkington and R. Durrett. Estimating tumor growth rates *in vivo*. *Bull. Math. Biol.*, 77(10):1934–1954, 2015.

[57] T. A. Traina, U. Dugan, B. Higgins, K. Kolinsky, M. Theodoulou, C. A. Hudis, and L. Norton. Optimizing chemotherapy dose and schedule by Norton-Simon mathematical modeling. *Breast disease*, 131:7–18, 2010.

[58] K. P. Wilkie and P. Hahnfeldt. Modeling the dichotomy of the immune responseto cancer: Cytotoxic effects and tumor-promotinginflammation. *Bull. Math. Biol.*, 79:1426–1448, 2017.